

Phenomenology of Tsunamis II: Scaling, Event Statistics, and Inter-Event Triggering

Eric L. Geist

U.S. Geological Survey, Menlo Park, CA, USA
egeist@usgs.gov

Contents

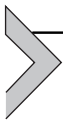
1. Introduction	36
1.1 Near-field Broadside Regime	37
1.2 Near-field Oblique Regime	37
1.3 Far-field Oblique Regime	37
2. Scaling	39
2.1 Local Run-up Heights	41
2.2 Tide-Gauge Amplitudes	49
2.3 Summary	55
3. Event Statistics	55
3.1 Source Size Statistics	57
3.2 Source Inter-event Time Statistics	62
3.3 Tsunami Size Statistics	64
3.4 Tsunami Inter-event Time Statistics	70
4. Inter-Event Triggering	73
4.1 Earthquake-to-earthquake Triggering	73
4.2 Earthquake-to-landslide triggering	75
4.3 Generalized Branching Process	76
5. Discussion	78
6. Summary	80
Acknowledgments	82
References	83

Abstract

Observations related to tsunami catalogs are reviewed and described in a phenomenological framework. An examination of scaling relationships between earthquake size (as expressed by scalar seismic moment and mean slip) and tsunami size (as expressed by mean and maximum local run-up and maximum far-field amplitude) indicates that scaling is significant at the 95% confidence level, although there is uncertainty in how well earthquake size can predict tsunami size ($R^2 \sim 0.4\text{--}0.6$). In examining tsunami

event statistics, current methods used to estimate the size distribution of earthquakes and landslides and the inter-event time distribution of earthquakes are first reviewed. These methods are adapted to estimate the size and inter-event distribution of tsunamis at a particular recording station. Using a modified Pareto size distribution, the best-fit power-law exponents of tsunamis recorded at nine Pacific tide-gauge stations exhibit marked variation, in contrast to the approximately constant power-law exponent for inter-plate thrust earthquakes. With regard to the inter-event time distribution, significant temporal clustering of tsunami sources is demonstrated. For tsunami sources occurring in close proximity to other sources in both space and time, a physical triggering mechanism, such as static stress transfer, is a likely cause for the anomalous clustering. Mechanisms of earthquake-to-earthquake and earthquake-to-landslide triggering are reviewed. Finally, a modification of statistical branching models developed for earthquake triggering is introduced to describe triggering among tsunami sources.

Keywords: Tsunami catalogs, Earthquake, Pareto size distribution, Power-law exponent



1. INTRODUCTION

In this second part of a comprehensive review of tsunami phenomenology, I examine earthquake and tsunami catalogs to determine relevant aspects of scaling, size and temporal distribution, and triggering. Unexpectedly large tsunamis relative to the magnitude of the causative earthquake are obviously of most concern to the hazard community. The focus on tsunami scaling in this chapter, therefore, relates to better understanding of the size distribution of tsunami amplitudes and the uncertainty of scaling relationships between earthquake potency and tsunami size. In examining tsunami catalogs, another unexpected behavior evident is clustering of tsunami events in time. This, in turn, is examined in this chapter by reviewing the inter-event time distribution and related triggering mechanisms associated with tsunamis and tsunami sources.

Part I of *Phenomenology of Tsunamis* (hereafter referred to as PT1, Geist, 2009) focused on tsunami events in isolation, in which observations related to the evolution of tsunamis, ranging from generation, propagation, and run-up, were systematically examined.

In PT1, tsunami generation was examined from the perspective of gauging the range of behaviors in terms of variations in earthquake slip patterns and landslide dynamics. Water-level observations were divided among three spatial regimes: near-field broadside (directly across the source), near-field oblique, and far-field. In each case, several hypotheses related to

these observations were formulated, to be tested as more data become available. These hypotheses are listed below.

1.1 Near-field Broadside Regime

Hypothesis 1 (Hyp. 1): For reasonably regular coasts, maximum offshore tsunami amplitude is most often associated with the first arrival, a non-trapped phase.

Hypothesis 2 (Hyp. 2): Strike-parallel distribution of maximum amplitude and run-up is significantly affected by fault slip heterogeneity.

Hypothesis 3 (Hyp. 3): Broadside run-up increases where high coseismic slip is located beneath deep water.

1.2 Near-field Oblique Regime

Hypothesis 4 (Hyp. 4): Maximum amplitude and run-up are most often derived from late arrivals resulting from the interaction of trapped phases (i.e., edge waves).

Hypothesis 5 (Hyp. 5): There exists a causal (but complex) relationship between fault slip heterogeneity and near-field oblique tsunami amplitude.

1.3 Far-field Oblique Regime

Hypothesis 6 (Hyp. 6): The deep-ocean far-field tsunami wavefield includes a well-developed coda caused by frequency dispersion, scattering, reflected, and refracted arrivals.

Hypothesis 7 (Hyp.7): Maximum amplitude and run-up at the coast from a far-field tsunami are derived from the complex interaction of the long tsunami coda and the excitation and resonance of trapped edge waves and shelf modes.

The analysis described in PT1 and for the most part in the present chapter is that of descriptive statistics, as distinguished from conceptual and engineering statistics, in the framework described by [Vere-Jones \(2010\)](#). In Section 4, conceptual statistics as it relates to a branching process for tsunami sources is briefly introduced. Engineering statistics as it relates to tsunami hazards is discussed by, for example, [Burroughs and Tebbens \(2005\)](#) and [Geist and Parsons \(2006\)](#).

Most of the research to date has focused on tsunamis as a deterministic phenomenon. As such, simulations of tsunamis critically rely on various scaling relationships to estimate seafloor motion and tsunami amplitude

from earthquake parameters measured from seismograms. For example, empirical scaling relations have been developed to determine tsunami amplitude from the moment magnitude (M_w) of the earthquake (e.g., Abe, 1995). Also, numerical models of tsunami propagations rely on initial conditions scaled from M_w and/or aftershock distributions. Little attention has been paid to understanding the uncertainty associated with the scaling relationships or the variation in possible tsunami outcomes for a fixed earthquake hypocenter and M_w .

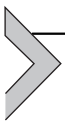
Much of this uncertainty is related to complexity in both the source process and the nearshore hydrodynamic response as the tsunami interacts with the coastal zone (e.g., Apotsos, Gelfenbaum & Jaffe 2012). Source complexity, particularly heterogeneity of the initial displacement field relative to the water depth, results in significant uncertainty in near-field scaling relationships. Anomalous tsunami earthquakes (Kanamori, 1972) highlight this fact, owing to their unusual occurrence near oceanic trenches. Similarly, the complexity of the far-field tsunami imparted by scattering during propagation and nearshore trapping and reflection results in a waveform in which the maximum amplitude is most often not associated with the direct arrival (Hyp. 4). Previous observations such as maximum amplitude increasing with increasing propagation distance for an event (Watanabe, 1972) appear counterintuitive when considering just the expected attenuation of the direct (unobstructed) phase of a tsunami.

In terms of temporal clustering, the least astonishing hypothesis of tsunamis, like earthquakes, is that they occur according to a Poisson process consisting of independent events. This itself, perhaps, leads to shorter than expected time between individual events compared to, for example, quasiperiodic inter-event distributions. Statistical evaluation of inter-event times for global tsunami sources indicates that there are more short inter-event times than even associated with a Poisson process (Geist & Parsons, 2008; Geist, Parsons, ten Brink, & Lee, 2009b). Certainly, aftershocks that are the primary cause of clustering in earthquakes can be tsunamigenic. However, a cursory examination of tsunami catalogs reveals that only a fraction of the over abundance of short inter-event times can be ascribed to aftershocks, suggesting other triggering relationships among tsunami sources.

The combination of scaling uncertainty and temporal clustering of tsunami sources can result in cases in which subsequent tsunamis related to earthquake aftershocks can be larger than the tsunami related to the main

shock. A classic example of this is documented by a sequence of earthquakes and tsunamis offshore of central Mexico in 1932. A $M=7.9$ – 8.1 main shock on June 3, 1932 along the Mexican subduction zone produced two tsunamigenic aftershocks: first, a $M=7.8$ event on June 18 (15 day inter-event time) and second, a $M=6.9$ event on June 22 (4 day inter-event time). The second aftershock generated a much larger local tsunami (10 m maximum run-up height) than either the main shock (3 m) or the first tsunamigenic aftershock (1 m) (Farreras & Sanchez, 1991). It is possible that the second aftershock triggered a landslide (or more likely, the landslide was triggered by loading from successive earthquakes: cf., Biscontin & Pestana, 2006) resulting in a larger tsunami than expected from its magnitude alone.

To outline the structure of this chapter, in Section 2 scaling of tsunami run-up heights and amplitudes with respect to earthquake magnitude and other source parameters is reviewed. These tsunami size scaling relationships are evaluated using standard regression techniques. In Section 3, the probability distribution of sizes and inter-event times are reviewed for both tsunami sources and tsunamis themselves. In presenting both phenomena, one can determine how closely tsunami statistics follow the statistics of their sources. Because there is no routine monitoring of landslides in terms of their size and occurrence, most of the review on scaling and event statistics will be focused on seismogenic tsunamis. In Section 4, triggering relationships that underlie temporal clustering of tsunami events are reviewed in more detail. In this section, a general branching model is introduced that can accommodate different sources (i.e., including landslides in a theoretical manner) and source statistics.



2. SCALING

Knowledge on how tsunami amplitude and run-up scale with different source parameters is particularly important for both tsunami hazard assessments and tsunami warning. It is reasonable to assume that there is a physical relationship between the size of the tsunami and the size of the causative earthquake, measured either by the mean fault slip or scalar seismic moment. For this reason, scaling is examined with respect to both local run-up heights and tide-gauge maximum amplitudes using regression analysis. Scaling in this sense is directly analogous to a large body of research into how peak seismic ground motion (displacement, velocity, and acceleration) scales

with earthquake source parameters. Peak ground displacement (PGD) is the closest seismic analog to maximum tsunami amplitude, although in practice displacement spectra derived from acceleration records are particularly sensitive to digitization errors and long-period noise (Faccioli, Paolucci, & Rey, 2004). As a simple example, using the mechanical definition of seismic moment ($M_0 = \mu A \bar{D}$, where μ is the shear modulus, A is the rupture area, and \bar{D} is the mean slip) and moment magnitude ($\log M_0 = (3/2)(M_w + 10.73)$), Yamada, Olsen, and Heaton (2009) indicate a linear scaling relationship between $\log(\text{PGD})$ and M_w . In the discussion below, I revisit the seismic ground-motion analog when interpreting the scaling of tsunami measurements to earthquake source parameters.

In the analysis that follows, the focus is on tsunamis generated from the inter-plate thrust earthquakes along subduction zones (Fig. 2.1), the most common mechanism for tsunamigenic earthquakes. By focusing on this fault type and not considering intra-plate earthquakes or tsunamigenic earthquakes from other plate-boundary faults, a direct line of inference can be made between fault rupture processes and tsunami measurements, without considering large variations in other factors such as focal mechanism. Of this dataset, two subgroups are considered: inter-plate thrust earthquakes that occur at typical seismogenic depths and tsunami earthquakes as defined by Kanamori (1972), and further elaborated by Kanamori and Kikuchi (1993) and Polet and Kanamori (2000) that generate much larger tsunamis relative to the magnitude of the causative earthquake. Tsunami earthquakes include slow tsunami earthquakes located near the trench of subduction zones and tsunami earthquakes that involve a triggered landslide component (Kanamori & Kikuchi, 1993). Because slow tsunami earthquakes occur at

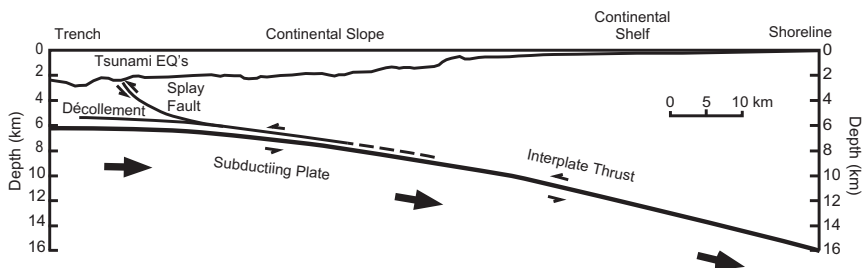


Figure 2.1 Schematic diagram of a continental subduction zone, indicating common faults that produce tsunamigenic earthquakes. Most earthquakes occur on the inter-plate thrust beneath the continental shelf and upper continental slope. Slow tsunami earthquakes are located beneath the lower continental slope near the trench.

very shallow depths within the subduction zones and seaward of the conventionally understood aseismic front (Byrne, Davis, & Sykes, 1988), the shear modulus is low and hence the rupture propagation speed of these earthquakes is also diagnostically low (Bilek & Lay, 1999). However, it is the large water depth above the rupture zone that is responsible for the higher than expected tsunami, rather than the rupture propagation speed. Slow tsunami earthquakes likely occur on the same inter-plate fault system, though they may occur on a subsidiary décollement or splay fault (Fukao, 1979) of that system (Fig. 2.1). Different earthquake parameters, including magnitude, geometric parameters of rupture zones, and statistics of coseismic slip, are used to establish the scaling relationships with local tsunami run-up heights (Section 2.1) and tide-gauge amplitudes (Section 2.2). These data were initially compiled by Lay, Kanamori, and Ruff (1982) and updated by Geist (2002) and in this study for more recent events.

2.1 Local Run-up Heights

Run-up measurements from high-water marks are typically made after a major tsunami by survey teams of international scientists. As indicated in PT1, there are a variety of water-level measurements made within the inundation zone, including flow depths relative to the local topographic elevation and run-up at the point of maximum inundation. Measurements are usually made relative to a vertical tidal datum at the time of the tsunami (Baptista, Priest, & Murty, 1993).

Because local run-up measurements are made at propagation distances typically within the characteristic source dimension of the earthquake, near-field scaling principally depends on the statistics of the seafloor displacement field. Tsunami propagation effects are minimal, although the effect of edge waves and site response (e.g., resonance) on scaling should not be overlooked. In the near-field broadside regime, the maximum water level through the duration of the tsunami at a coastal location (i.e., the quantity measured in the field) is typically associated with the direct arrival (Hyp. 1 described in the Introduction). Therefore, the spatial average and maximum run-up along the coastline can be directly related to the initial offshore displacement field. In the near-field oblique regime, the relationship between the initial offshore displacement field and the spatial statistics of run-up is more complex, owing to the effects of edge waves (Hyp. 4 and Hyp. 5).

Unfortunately, the initial offshore displacement field is rarely measured. Instead, we examine possible scaling relationships between run-up and

earthquake source parameters that are estimated by seismological methods. In the study by Geist (1999), the amount and distribution of slip on the fault have the largest control on the displacement field. Other fault geometry parameters listed in the finite-source catalog, such as rupture width, depth, and fault dip, as well as physical properties such as shear modulus, have secondary effects. It is, therefore, logical to first examine how near-field run-up scales with mean slip (Fig. 2.2). In this and subsequent figures, both inter-plate thrust earthquakes that occur at typical seismogenic depths (solid circles) and anomalously shallow tsunami earthquakes (open squares) are displayed as separate events.

A statistical test is performed to determine whether the scaling of run-up with slip and other parameters listed below is significant. The null hypothesis in this case is that there is no scaling (zero slope in the regression line, given the available data). The p -value is the probability that the estimated scaling could be obtained by random chance (i.e., the null hypothesis is true). For this study, $p < 0.05$ is chosen from the outset to determine whether scaling effects are significant. The p -value does not indicate the magnitude of scaling

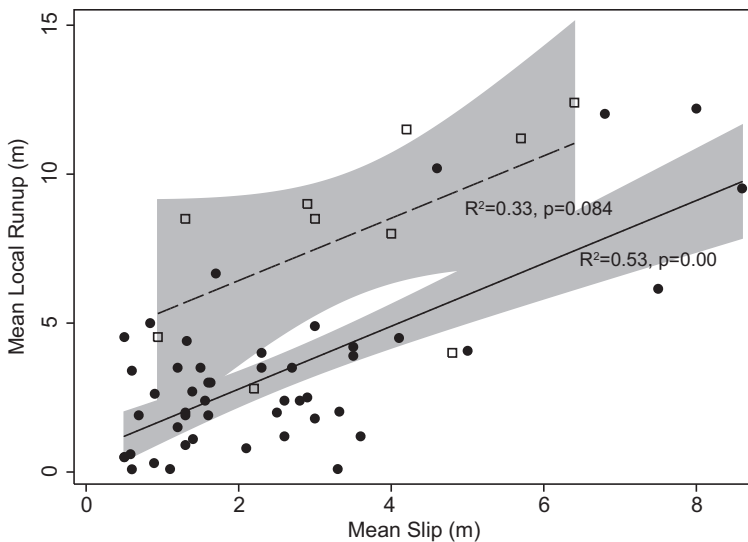


Figure 2.2 Plot of mean near-field run-up relative to mean slip of the causative earthquake. Solid circles: inter-plate thrust earthquake at typical seismogenic focal depths (solid regression line). Open squares: shallow tsunami earthquakes (dashed regression line). Shaded region around each regression line indicates 95% confidence interval of the mean.

(slope) nor how well source parameters such as slip predict run-up as measured by the coefficient of determination (i.e., square of the sample correlation coefficient R^2). For the example shown in Fig. 2.2, although the scaling of mean local run-up with mean slip appears to be similar for both tsunami and inter-plate thrust earthquakes, the p -value for the tsunami earthquake subset is 0.084, indicating that scaling is not significant.

The large scatter in the plot, as measured by R^2 and the shaded regions indicating the 95% confidence interval of the mean, in part has to do with uncertainty in how slip is determined. For many large subduction zone earthquakes, inversion of seismic waveforms provides information on the slip distribution. Some of the problems associated with seismic inversions have been discussed by Beresnev (2003), Bos and Spakman (2003), Das and Suhadolc (1996), and Page, Custódio, Archuleta, and Carlson (2009). These studies indicate that while gross features of inverted slip distributions may be stable among different parameterizations and inversion techniques, fine-scale features may be dependent on the inversion technique used.

Other earthquake parameters that may be measured with more precision than slip can be evaluated in terms of scaling with tsunami size. There has been significant discussion in the past regarding how average slip scales with the dimension of the rupture zone for large earthquakes, i.e., as the rupture width saturates for inter-plate thrust earthquakes. This transition occurs for $M_w \geq 7.0 - 7.5$ earthquakes, approximately the same as the minimum magnitude necessary for generating an observable tsunami (Ward, 1980). For these large earthquakes, conceptually the entire brittle portion of the crust is ruptured in the dip direction and the width of rupture no longer increases with seismic moment. Two popular models that have been proposed include (a) the W -model in which slip scales with fault width and is, therefore, constant for large earthquakes (i.e., $M_0 \propto L$) (e.g., Romanowicz, 1994) and (b) the L -model in which slip scales with fault length and, therefore, increases with seismic moment for large earthquakes (i.e., $M_0 \propto L^2$) (e.g., Scholz, 1994). More recent studies suggest a more complicated scaling relationship between slip and fault length. Liu-Zeng, Heaton, and DiCaprio (2005) indicate that slip-length scaling is dependent on the level of slip heterogeneity (e.g., as measured by a spectral decay constant in the wave number domain) and that scaling is approximately linear only for smooth slip distributions. Shaw and Scholz (2001) indicate that there is a gradual decrease in the \bar{D}/L ratio with increasing M_w , but with significant scatter, tending toward constant slip only for very long ruptures ($L/W > 10$). They suggest that dynamic effects, in particular dynamic energy concentrations that take

very long distances to build up and to die out, are responsible for the complex scaling relationship. In a statistically rigorous analysis, Kagan (2002b) examines the scaling between aftershock length and seismic moment and finds no break between small and large earthquakes (i.e., $M_0 \propto L^3$) up to $M_w = 8.4$ (the largest magnitude in his analysis of earthquakes occurring in the years 1977–2000). This implies that larger earthquakes have a larger stress drop than smaller earthquakes, or, more likely, that ruptures for large earthquakes propagate below typical seismogenic depths (cf., Shaw & Wesnousky, 2008).

Figure 2.3 shows the scaling of mean local run-up as a function of rupture length. Run-up from typical inter-plate thrust earthquakes exhibits a similar scaling with length as with mean slip (Fig. 2.2). The variation of run-up with length shown in Fig. 2.3 is interpreted as an indirect dependence on fault slip according to the L -model. For tsunami earthquakes, however, there is no significant scaling ($p = 0.76$), likely related to the small range in rupture lengths included in the tsunami earthquake dataset. The lack of scaling may also reflect unusual mechanical properties of tsunami earthquakes or possible distance attenuation effects, since tsunami

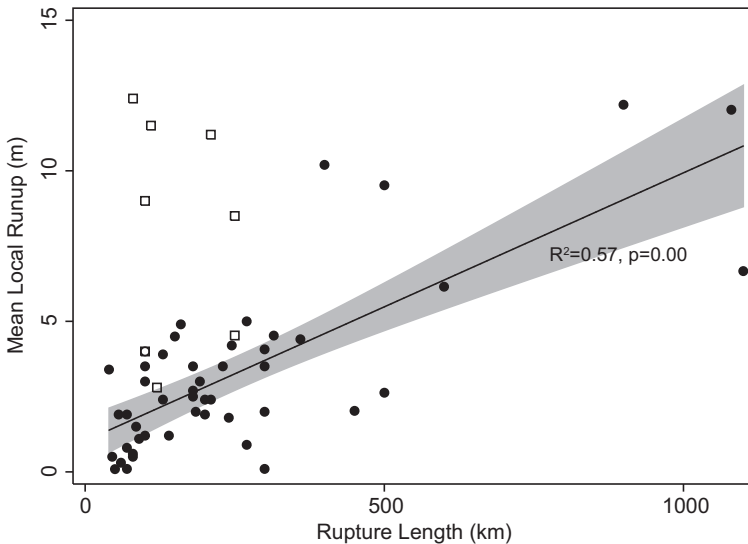


Figure 2.3 Plot of mean near-field run-up relative to the rupture length of the causative earthquake. Solid circles: inter-plate thrust earthquake (solid regression line). Open squares: shallow tsunami earthquakes (no regression line). Shaded region around each regression line indicates 95% confidence interval of the mean.

earthquakes occur farther offshore than typical inter-plate thrust earthquakes. Scaling of mean run-up with respect to rupture area (not shown) is similar to the length scaling results shown in Fig. 2.3, in terms of p -value and R^2 . There does not appear to be significant scaling of mean run-up with respect to rupture width or aspect ratio (i.e., $p > 0.05$ in both cases).

An alternative to scaling with respect to slip (or indirectly with respect to rupture length as described above) is to scale near-field run-up with respect to seismic moment. Because observed values of seismic moment are routinely calculated from the inversion of broadband seismic waveforms (Dahlen & Tromp, 1998; Dziewonski, Chou, & Woodhouse, 1981), seismic moment catalog values are more certain than slip distributions. If we initially assume that local run-up does not significantly scale with rupture width or length in the mechanical definition of seismic moment ($M_0 = \bar{\mu} \bar{D}_s L W$), then scaling of run-up with respect to slip is equivalent to scaling with respect to seismic moment. However, the self-similar nature of rupture means that slip and fault dimensions scale together with the size of the earthquake. In addition, increasing the dimensions of the rupture zone results in an increase in the volume of water initially displaced. Therefore, log-log regressions of scaling with respect to seismic moment (i.e., power model) are investigated. Referring back to the strong ground-motion analogy introduced previously, PGD also scales with seismic moment in a log-log relationship. For example, Yamada et al. (2009) suggest that for small earthquakes, where the rupture area is approximately the square of the rupture length, $\log \text{PGD} \propto (1/2)M_w$ and for large earthquakes, where the rupture width is saturated, $\log \text{PGD} \propto (3/4)M_w$. Along a similar line of reasoning, Faccioli et al. (2004) used the far-field displacement expression of Brune (1970) as a function of the static stress drop ($\Delta\sigma$), to establish a linear scaling of $\log \text{PGD} \propto M_w$.

The corresponding plot of mean local run-up with respect to M_w is shown in Fig. 2.4. Some of the scatter for typical inter-plate thrust earthquakes is caused by variable water depth above regions of high slip that have a significant effect on local run-up (Hyp. 3). For typical inter-plate thrust earthquakes, there is also significant scatter in the scaling relation caused by heterogeneity in the source processes (Geist, 2002). Earthquakes like the 1960 Chile earthquake and the 2005 Sumatra earthquake are deficient at tsunami generation relative to their magnitude, owing to most of the slip being toward the down-dip extent of rupture (in shallow water or below land). In contrast, tsunami earthquakes (solid circles in Fig. 2.4) are typically associated with higher run-up and have less uncertainty in the scaling

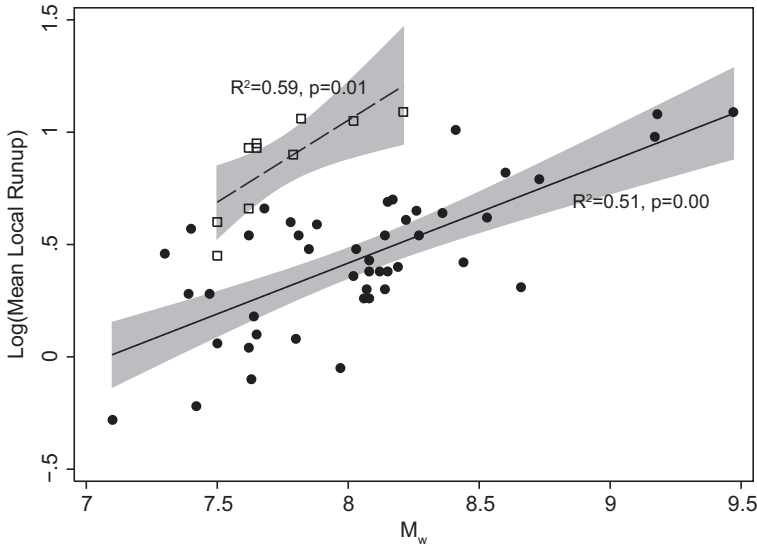


Figure 2.4 Plot of mean near-field run-up relative (logarithmic scale) to the moment magnitude (M_w) of the causative earthquake. Solid circles: inter-plate thrust earthquake (solid regression line). Open squares: shallow tsunami earthquakes (dashed regression line). Shaded region around each regression line indicates 95% confidence interval of the mean.

relationship with respect to M_w compared to typical inter-plate thrust earthquakes and compared to scaling with respect to slip (Fig. 2.2). Because vertical coseismic displacement accompanying these earthquakes is generally restricted to deeper water, their amplitude and wave number increase substantially during propagation toward shore, according to Green's law (Hyp. 3). Although there are only a few observations of tsunamis from outer-rise earthquakes, because these events too occur in deep water, the associated run-up is generally higher than typical inter-plate thrust earthquakes for a given magnitude.

The previous discussion focused on scaling of mean local run-up for an event. However, scaling of maximum local run-up R_{\max} is of particular interest, both in terms of assessing tsunami hazards and with respect to the Imamura–Iida definition of tsunami intensity (cf., Satake, 2007): $I = \log_2 R_{\max}$. Shown in Fig. 2.5 is a plot of maximum run-up relative to M_w . Maximum run-up associated with an event is sensitive to slip/water depth variations and the nearshore hydrodynamic response as discussed in Chapter 3 of PT1. There is a surprisingly high coefficient of determination

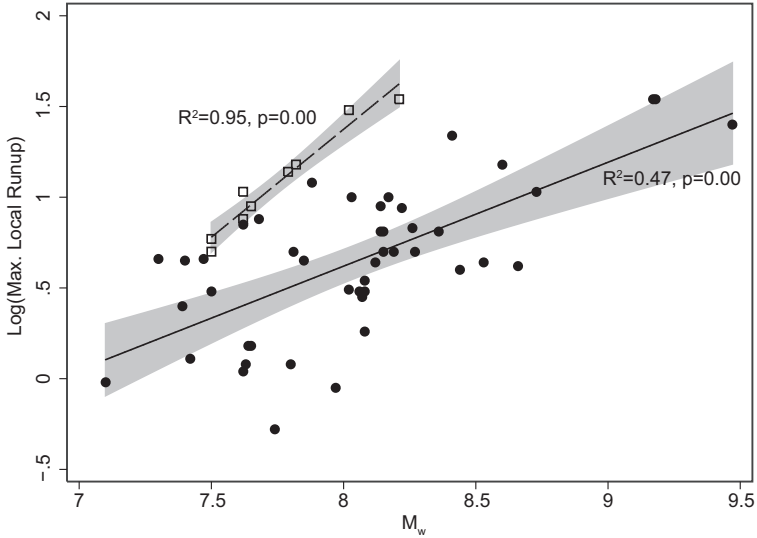


Figure 2.5 Plot of maximum near-field run-up (logarithmic scale) relative to the moment magnitude (M_w) of the causative earthquake. Solid circles: inter-plate thrust earthquake (solid regression line). Open squares: shallow tsunami earthquakes (dashed regression line). Shaded region around each regression line indicates 95% confidence interval of the mean.

($R^2 = 0.95$) for tsunami earthquakes, considering that R_{\max} is a statistically less stable measure than the mean run-up. The strong scaling with respect to M_w is consistent with the interpretation that tsunami earthquakes occur within a restricted dip position along the plate-boundary thrust, thus limiting the variation in the overlying water depth.

Statistically, estimation of maximum run-up from an event is dependent on the sample size of run-up measurements from that event. One can examine maximum run-up with respect to the lognormal spatial distribution of run-up proposed by Choi, Hong, and Pelinovsky (2006) and Choi, Pelinovsky, Ryabov, and Hong (2002), with probability density

$$f(R) = \frac{1}{R\sigma\sqrt{2\pi}} \exp\left[-\frac{(\ln(R) - \mu)^2}{2\sigma^2}\right], \quad [2.1]$$

where μ and σ are the mean and standard deviation of $\ln(R)$, respectively. Assuming that near-field run-up is globally represented by a lognormal distribution, a central question is whether a random run-up sample from post-tsunami field measurements is adequate in estimating the maximum

run-up for an event. For a given number of run-up measurements N , probability density of measuring R_{\max} in N samples is given by

$$g(R_{\max}) = N[F(R)]^{N-1}f(R), \quad [2.2]$$

where F is the cumulative distribution function (Kempthorne & Folks, 1971). Fig. 2.6 shows the probability density of the maximum measured run-up for the case of the $M_w = 7.8$ 1994 Java tsunami earthquake. To calculate this figure, the distribution parameters of Eqn [2.1] are estimated using the maximum-likelihood method and the data described by Tsuji et al. (1995) ($N = 62$). The most likely maximum run-up indicated in Fig. 2.6 is 11.8 m. This compares to the observed maximum of 13.9 m, which is within the 95% confidence range of the distribution (9.3–16.4 m). As indicated previously, the mean run-up (i.e., $\exp(\mu + \sigma^2/2)$) from the sample of post-tsunami field measurements approximately scales with M_w (Fig. 2.4). It is important to take sample size into consideration when interpreting plots such as Fig. 2.5: i.e., scaling of R_{\max} with respect to M_w may be subject to varying uncertainty, owing to the large variation in run-up sample numbers for each tsunami.

Finally, because tsunami earthquakes ostensibly occur on the same fault system as typical inter-plate thrust earthquakes (Fig. 2.1), it is useful to determine whether the scaling relations discussed in this section are significantly different. To do this, a Wald test is used on the regression results for each subgroup of earthquakes. For scaling of mean run-up with respect to slip, the two subgroups are not significantly different at the 95% confidence

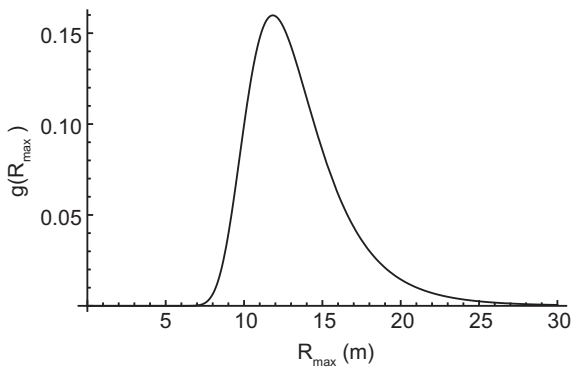


Figure 2.6 Probability density of maximum observed run-up for the 1994 Java tsunami earthquake, assuming a lognormal run-up distribution. *Parameter estimation based on data from Tsuji et al. (1995).*

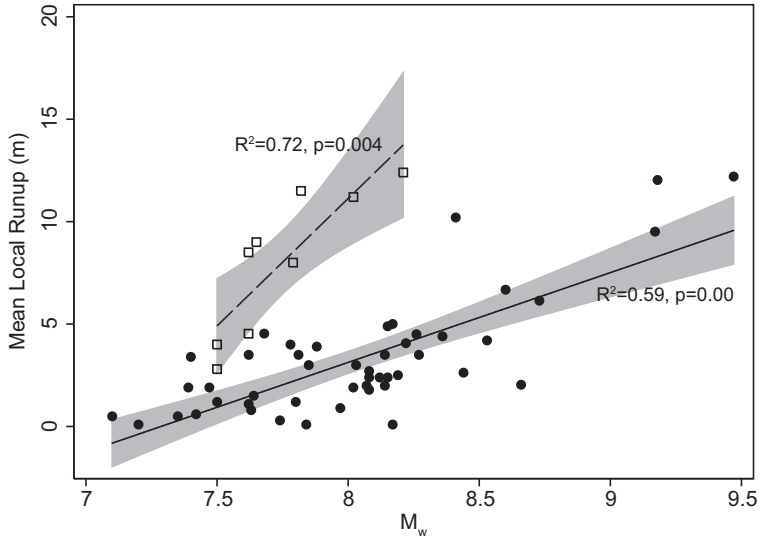


Figure 2.7 Plot of mean near-field run-up relative (linear scale) to the moment magnitude (M_w) of the causative earthquake. Solid circles: inter-plate thrust earthquake (solid regression line). Open squares: shallow tsunami earthquakes (dashed regression line). Shaded region around each regression line indicates 95% confidence interval of the mean.

interval (Fig. 2.2). As mentioned previously, this may be due to the large uncertainty in slip inversion results. For scaling of logarithmic run-up with respect to moment magnitude (logarithm of scalar seismic moment), the two subgroups are significantly different for maximum run-up (Fig. 2.5), but not for mean run-up (Fig. 2.4). This is likely because of the limited number of tsunami earthquakes in the catalog. If instead linear scaling of run-up with respect to moment magnitude is regressed, the two subgroups are significantly different for both mean and maximum run-ups (Figs 2.7 and 2.8). Linear scaling, however, does not conform to a power model as expected from physical relationships described above and plots of the residuals suggest a nonlinear relationship in each case.

2.2 Tide-Gauge Amplitudes

Far-field tsunamis are most often recorded by tide gauges (time-series measurements). Thus, in contrast to run-up measurements that are recorded by post-event surveys and represent the highest onshore water level over the duration of a tsunami, tide-gauge records are instrumental amplitude

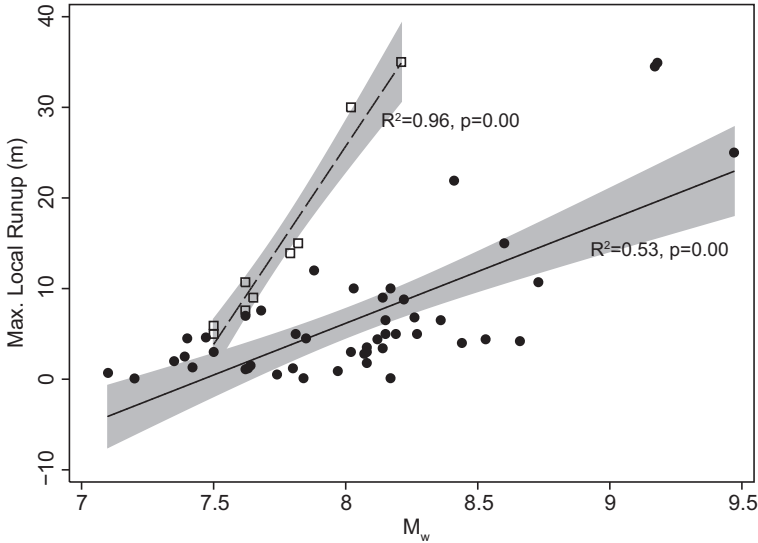


Figure 2.8 Plot of maximum near-field run-up (linear scale) relative to the moment magnitude (M_w) of the causative earthquake. Solid circles: inter-plate thrust earthquake (solid regression line). Open squares: shallow tsunami earthquakes (dashed regression line). Shaded region around each regression line indicates 95% confidence interval of the mean.

measurements taken during the event and record the complete tsunami waveform. The typical tsunami marigram is best described as a direct arrival followed by a coda that encompasses multiple reflections, scattering, near-shore response, and harbor resonance (Fig. 2.9). PT1 discusses the waveform statistics of the tsunami coda that can be represented by an exponentially decaying Gaussian waveform. Scaling of far-field tsunamis is referenced to the maximum tsunami amplitude (a_{\max}) of the tsunami waveform—most often this occurs after the first arrival but near the beginning of the coda (i.e., within one e -folding time) (Fig. 2.9).

Much of the spatially varying details of the initial tsunami displacement field are attenuated at far-field distances, such that a point-source representation and scaling relationships based on $\log(M_0)$ or moment magnitude M_w can be used. Several authors have indicated that $\log(a_{\max})$ scales with M_w (Abe, 1995; Comer, 1980; Okal, 1988; Pelayo & Wiens, 1992), although there is some discussion as to the correct constant of proportionality (i.e., slope). Because $M_w = (2/3)\log M_0 - 10.7$, assuming a linear scaling between $\log(a_{\max})$ and $\log(M_0)$ implies a slope of 3/2 in the scaling of \log

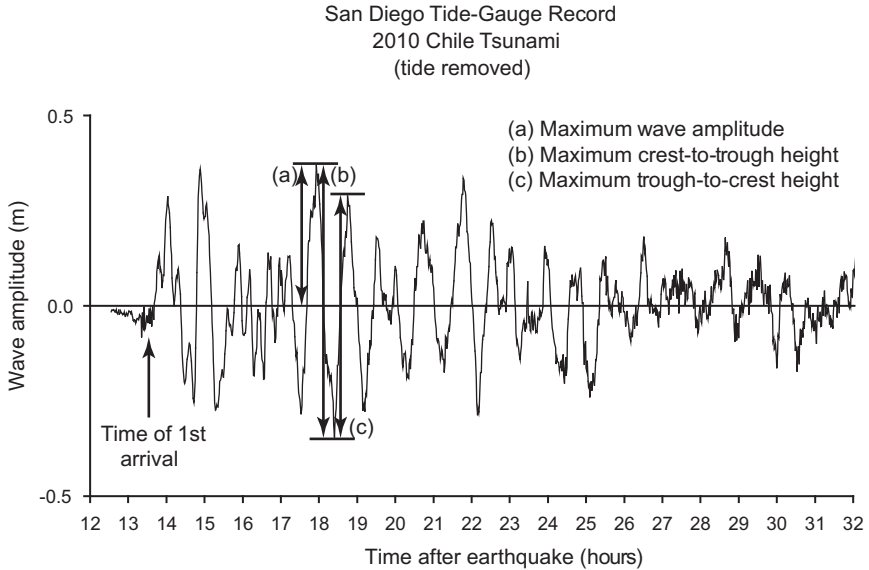


Figure 2.9 Time-series recording at the San Diego tide-gauge station of the tsunami generated by the $M_w = 8.8$, February 27, 2010 Chile earthquake.

(a_{\max}) with respect to M_w (Abe, 1995; Pelayo & Wiens, 1992). From theoretical considerations, Comer (1980) indicates that the $\log(a_{\max}):M_w$ slope should be $4/3$, neglecting dispersion, and that the $3/2$ slope is only applicable at the highly dispersive limit. Pelayo and Wiens (1992) indicate that the empirical best fit of data from 1943 to 1987 is a linear slope between $\log(a_{\max})$ and M_w . This is less than the theoretically expected slope and suggests that the efficiency of tsunami generation decreases with increasing M_0 (Pelayo & Wiens, 1992). This may be consistent with large earthquakes, such as 1964 Alaska and 1960 Chile in which a portion of the rupture extends beneath land, rather than being restricted to the submarine realm.

In past scaling studies, distance attenuation is accounted for using a geometrical spreading factor of $|\sin(\Delta)|^{1/2}$, where Δ is angular distance that originated from seismic surface wave theory (Dahlen & Tromp, 1998; Okal, 1988; Pelayo & Wiens, 1992). One has to be careful in applying this factor to tsunamis at long distances, owing to the fact that unlike seismic surface waves, tsunamis are obstructed by landmasses during global propagation. Distance attenuation is also accounted for by a $\log(D)$ constant in Abe's scaling relations, where D is linear distance (km) (e.g., Abe, 1995): $\log(a_{\max}) = M_w - \log D - 5.55 + C$. The constant C is zero for tsunamis generated in the forearc (inter-plate thrust) and 0.2 for back-arc tsunamis.

Travel time attenuation is likely a more accurate correction (cf., Eqn [38] in PT1), although tsunami catalogs do not routinely record this parameter.

Scaling relationships were examined for 20 Pacific tide-gauge stations using data from 1877 to 2010 and corrected using the $|\sin(\Delta)|^{1/2}$ geometrical spreading factor. Figure 2.10 shows four mid-ocean tide-gauge stations that are representative samples of the scaling relationships. In almost all cases, scaling of $\log(a_{\max})$ with M_w is significant ($p < 0.05$), with the exception being the Papeete tide-gauge station. The abundance of maximum amplitude values of 0.1 m is interpreted as the minimum detection limits for analog tide-gauge records (e.g., Hilo station in Fig. 2.10). A left-censored regression is performed to take into account this detection limit as shown by the solid lines in Fig. 2.10 (dashed lines represent ordinary linear regression). This expanded examination of tide-gauge records and the left-censored regression suggests that the slope between $\log(a_{\max})$ and M_w is less than one for all stations, although the slope is nearly one for the Hilo station. Thus, all stations exhibit a slope less than theoretical values (Abe, 1995; Comer, 1980). The coefficient of determination ranges from $R^2 = 0.1$

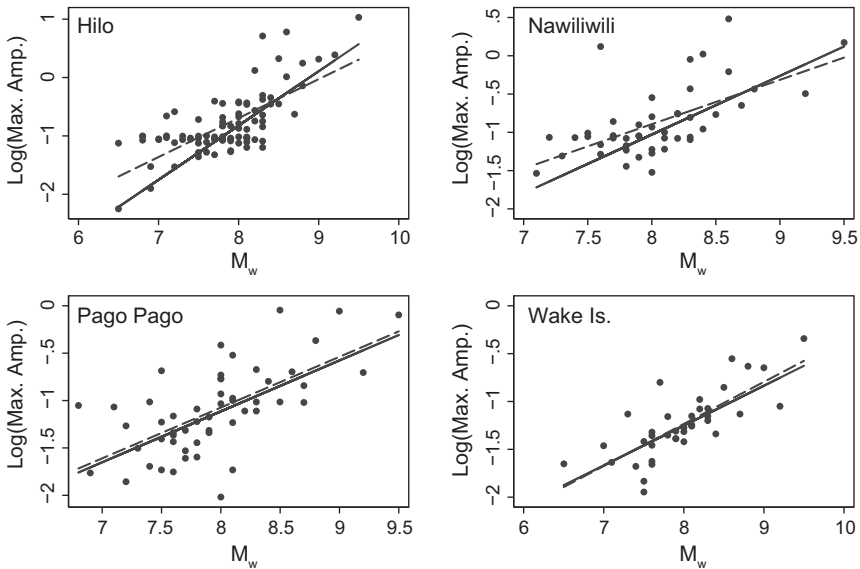


Figure 2.10 Plots of maximum tsunami amplitude (logarithmic scale) relative to the seismic moment of the causative earthquake at four representative mid-ocean tide-gauge stations. Amplitudes have been scaled by a factor of $|\sin(\Delta)|^{1/2}$. Dashed line represents ordinary regression; solid line represents censored regression (0.1 m amplitude values).

(Pago Pago) to $R^2 = 0.6$ (Wake Island). Differences in the residuals among the tide-gauge stations are likely due to site/island response (cf., van Dorn, 1984; Rabinovich, 1997).

The distance attenuation factor is subject to some further scrutiny for the simple fact that the maximum amplitude often occurs in the coda and is, therefore, affected by the combination of the source radiation pattern, scattering, reflections, and the nearshore response (PT1, Chapter 4). Watanabe (1972) classified tide-gauge records of four trans-Pacific tsunamis (1952 Kamchatka, 1957 Aleutian, 1960 Chile, and 1964 Alaska) according to the length and nature of the coda (the latter, in terms of the number of coda wave groups or packets: 1, 2, or 3). Interestingly, the data from the Watanabe (1972) study indicate that the maximum amplitude of wave groups in the coda does not obviously decrease with travel time in the far-field and may even increase for some events, using a linear attenuation relationship. It is not clear that the first, second, and third wave groups have a common origin for different tide-gauge locations. Watanabe (1972) indicates that the overall maximum amplitude for the entire time series tends to show a small decrease with travel time, except for ray paths between Kamchatka and Chile. Here, the Watanabe (1972) study is revised by examining the maximum amplitude of 10 transoceanic tsunamis (1952 Hokkaido, 1952 Kamchatka, 1957 Aleutian, 1960 Chile, 1963 Kuril, 1964 Alaska, 1965 Aleutian, 2003 Hokkaido, 2004 Sumatra, and 2010 Chile). Representative events that include near-field measurements are shown in Fig. 2.11 (1952 and 2003 Tokachi-Oki, 1964 Alaska, and 2010 Chile). In each case, attenuation is inferred from the data, using either $|\sin(\Delta)|^{-1/2}$ (line in Fig. 2.11) or $\log(D)$ functions. There is substantial scatter for all transoceanic tsunamis, with R^2 ranging from 0.50 (1964 Alaska) to 0.73 (2003 Tokachi-Oki). Variations in R^2 appear to be related to the number of near-field measurements available for an event. For all cases examined where there is sufficient near-field data, attenuation of the maximum amplitude with travel time is evident. It is likely that cases in which Watanabe (1972) inferred that maximum amplitude did not attenuate with travel time (e.g., the 1960 Chile tsunami) were biased by the lack of near-field records.

Because the maximum amplitude occurs late in the wave train (Fig. 2.9) and not with the direct arrival, the physical link between M_0 as a measure of overall potency of seafloor displacement and maximum tsunami amplitude at a far-field recording station is not immediately clear. Past theoretical determinations of M_0 -amplitude scaling are derived for the direct arrival and do not include the effects of scattering and multiple reflections. For the

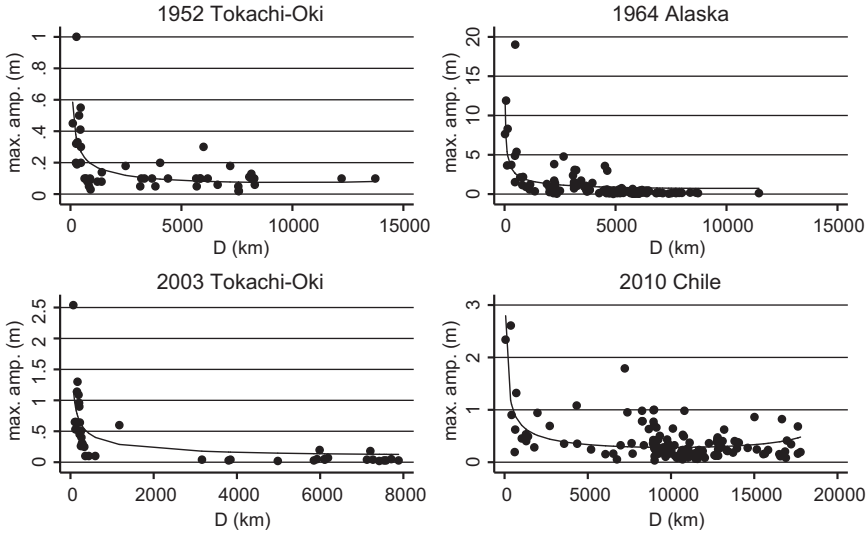


Figure 2.11 Plots of maximum tsunami amplitude recorded at coastal tide-gauge stations relative to source–receiver distance (km) for four transoceanic tsunamis generated by large inter-plate thrust earthquakes with near-field measurements. Line represents nonlinear regression fit of $|\sin(\Delta)|^{-1/2}$ function.

strong ground-motion analog that exhibits similar wave train characteristics, Boore (1983) developed a procedure using classical equations from random vibration theory. For a given waveform and assuming stationarity, Cartwright and Longuet-Higgins (1956) indicate that the asymptotic expression that relates the expected value of the largest amplitude $E(a_{\max})$ to the rms amplitude a_{rms} is given by

$$\frac{E(a_{\max})}{a_{\text{rms}}} = [2 \ln(N)]^{1/2} + \gamma [2 \ln(N)]^{-1/2}, \quad [2.3]$$

where N is the number of waves (i.e., extrema) and γ is Euler’s constant (see also Udvardi & Trifunac, 1974). The rms amplitude of the tsunami waveform is more clearly related to the source potency of the earthquake than the maximum amplitude. Boore (1983) determined the duration T from an evaluation of the corner frequency (cf., Fig. 30 in PT1): $T = f_c^{-1}$. N is then determined from $N = 2f_0 T$, where f_0 is the dominant frequency. For large N , the most probable maximum amplitude $\mu(a_{\max})$ is given by (Longuet-Higgins, 1952):

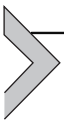
$$\frac{\mu(a_{\max})}{a_{\text{rms}}} = [2 \ln(N)]^{1/2}. \quad [2.4]$$

However, the amount of data needed to estimate $\mu(a_{\max})$ for tsunamis necessarily involves the portion of the waveform that includes the exponentially decaying coda (i.e., nonstationary). Therefore, Eqn [2.3] is most appropriate for tsunami data.

2.3 Summary

For typical inter-plate thrust earthquakes, local run-up scales with the primary tsunami generation parameter: mean coseismic slip. There also exists a significant log-log scaling relationship between the scalar seismic moment and mean and maximum local run-up. For tsunami earthquakes, there are currently too few events in the historical catalog to confirm a slip-run-up scaling relationship (at the 95% confidence level), although a moment-run-up scaling relationship for tsunami earthquakes can be firmly established. In addition, one cannot separate tsunami earthquakes as a distinct subset from typical inter-plate thrust earthquakes, except for maximum run-up statistics. Overall, however, the trend in the available observations suggests that tsunami earthquakes result in higher local run-up than inter-plate thrust earthquakes, for a given seismic moment. The origin of the uncertainties present in the aforementioned scaling relations is most surely related to observational errors, though in general, uncertainty related to the natural complexity of the physical processes involved cannot be ruled out (cf., Vere-Jones, 2010).

When corrected for geometric spreading, maximum tsunami amplitudes measured on far-field tide-gauge stations also scale with seismic moment on log-log plots. The R^2 values for far-field scaling are similar to those for near-field run-up measurements. Past theoretical scaling relationships of $\log(a_{\max})$ as a function of M_w predicted slopes greater than one, whereas the observed scaling relationships for 20 Pacific tide-gauge stations indicate slopes less than or equal to one. Although effects of source complexity are likely attenuated in the far-field, variability in the tsunami wavefield caused by reflections and scattering during open-ocean propagation in addition to the site response near the recording station conspire to cause of the lower than expected scaling slope. These effects are also expressed by variation of the maximum amplitude arrival within the tsunami wave train (discussed in detail in Section 4 of PT1).



3. EVENT STATISTICS

Although there are several descriptive statistical measures of earthquake and tsunami catalogs, in this section, I focus on the salient research

describing the size distribution and inter-event distribution of sources (primarily earthquakes in Sections 3.1 and 3.2) and tsunamis (Sections 3.3 and 3.4). We would expect the statistics of tsunamis to be similar to that of earthquakes. However, only earthquakes under certain conditions generate observable tsunamis: if the magnitude is large enough, if the earthquakes (or triggered landslides) are beneath the ocean, and if the earthquakes are not very deep. These conditions select a subset of all possible earthquakes and it is worth investigating whether the same statistical models of seismicity apply to tsunamis under these conditions.

The size distribution of the causative sources for tsunamis and tsunamis themselves are analyzed in the framework of a modified power-law or “Pareto” distribution, the latter named after the engineer and economist Vilfredo Pareto (1848–1923) (Clark, Cox, & Laslett, 1999; Kagan, 2002a; Newman, 2005). For earthquakes, the Pareto distribution forms the basis for the well-known Gutenberg–Richter (G–R) relation that relates the frequency of earthquake occurrence to earthquake magnitude.

In analyzing the inter-event distribution, both tsunami sources and tsunamis are viewed as point processes in which each point represents the time and location of an event (Schoenberg, Brillinger, & Guttorp, 2002). Because tsunamis can propagate to extremely far distances from the source and can persist for long times (e -folding times of 22 h at the coast, PT1), at first glance it seems difficult to directly apply point-process theory that has been established for earthquakes to analyze tsunamis. However, because the overall mean return time for tsunamis, either globally or at a particular recording station is long relative to the event duration, a point-process description is still applicable (Corral, 2009). Even for tsunamis occurring close in time relative to the e -folding time, it still is possible to distinguish individual events at individual recording stations as described in Section 3.4.

Although attempts have been made to compile tsunami observations over several centuries, or even millennia (Gusiakov, 2001), instrumental observations have only been available over approximately the last century. Even considering only the instrumental tsunami catalog, issues such as measurement errors, censoring, catalog completeness, and under-sampling need to be considered. Geist et al. (2009b) describe instrumental censoring in which smaller tsunamis are difficult to identify on analog records and in the presence of ambient noise, as well as geographic censoring in which tsunamis that occur where there is a lack of instrumental coverage are also not identified. Because of censoring effects, catalog completeness becomes an important issue for analyzing smaller tsunamis. In addition, even over

a century, a tsunami catalog may be of insufficient duration to capture the largest events that have mean return times of hundreds to thousands of years. Examples include large earthquakes along the Cascadia (Atwater & Hemphill-Haley, 1997) and Sumatra–Andaman subduction zones (Jankaew et al., 2008). Catalog completeness is therefore also a significant issue that one needs to be aware of.

3.1 Source Size Statistics

The G-R relation is commonly referred to when discussing earthquake size distributions. This relation is a magnitude–frequency relation usually given in cumulative form: $\log N(m) = a - bm$, where $N(m)$ is the number of earthquakes with magnitude $\geq m$ (Kagan, 2002a; Utsu, 2003). Strictly speaking, the G-R relation does not define a statistical distribution (Vere-Jones, 2010); moreover, fitting observed data to this relation cannot be performed using standard regression methods (Greenhough & Main, 2008; Leonard, Papasouliotis, & Main, 2001; Vere-Jones, 2010). Kagan (2002a) indicates that the density distribution that forms the basis of the G-R relation is a Pareto distribution:

$$\varphi(M) = \beta M_t^\beta M^{-1-\beta} \quad \text{for } M_t \leq M, \quad [2.5]$$

where the power-law exponent of the density distribution (β) is related to the b -value in the G-R relation by $\beta = (2/3)b$ and M_t is the minimum threshold seismic moment for catalog completeness.

Because of source finiteness in the Earth, the above distribution (Eqn [2.5]) cannot increase to indefinite magnitude. Various distributions that comply with source finiteness have been proposed, as summarized by Kagan (2002a). These include modified Pareto distributions in which the cumulative and density forms are sharply truncated (termed characteristic and truncated G-R, respectively) or gradually tapered (termed tapered G-R and gamma distributions, respectively). The gamma distribution is perhaps most consistent with the observed data and finite total seismic energy release (Greenhough & Main, 2008; Main, 2000b; Sornette & Sornette, 1999). The form of the gamma distribution given by Kagan (2002a) is

$$\varphi(M) = C\beta \frac{M_t^\beta}{M^{1+\beta}} \exp\left(-\frac{M_t - M}{M_c}\right) \quad \text{for } M_t \leq M < \infty, \quad [2.6]$$

where C is a normalization constant and M_c is the corner seismic moment, beyond which the distribution decays much faster than the Pareto

distribution (Eqn [2.5]) as shown by comparing the complementary cumulative distribution functions $\Phi(M)$ in Fig. 2.12.

Parameter estimation for the modified G-R relation and earthquake size distributions (e.g., Eqn [2.6]) has been performed for the global catalog as well as different geographic zonation schemes, such as Flinn–Engdahl zonation (Kagan, 1997, 1999, 2002c). Among the findings from these studies is the nearly constant value of $\beta = 0.60\text{--}0.66$ for nearly all seismic zones. A later study (Bird & Kagan, 2004) compared the parameters of earthquake size distributions among different tectonic plate-boundary types (subduction, mid-ocean ridges, etc.). While the power-law exponent β is consistent among different plate-boundary types, the corner moment M_c varies considerably. Bird and Kagan (2004) used a maximum-likelihood technique to determine the expected corner moment M_c and log-likelihood contours in $\beta\text{--}M_c$ space to determine the 95% confidence limits. For subduction zones, where most tsunamis are generated, the corner magnitude m_c corresponding to M_c is $m_c = 9.58$, with a lower 95% confidence limit of $m_c = 9.12$. The upper confidence limit is unknown, owing to an insufficient number of earthquakes with $M > M_c$ in the historical catalog. For any particular plate-boundary type, Kagan (2002c) indicates that M_c does not appear to depend on a geographic region or strain rate.

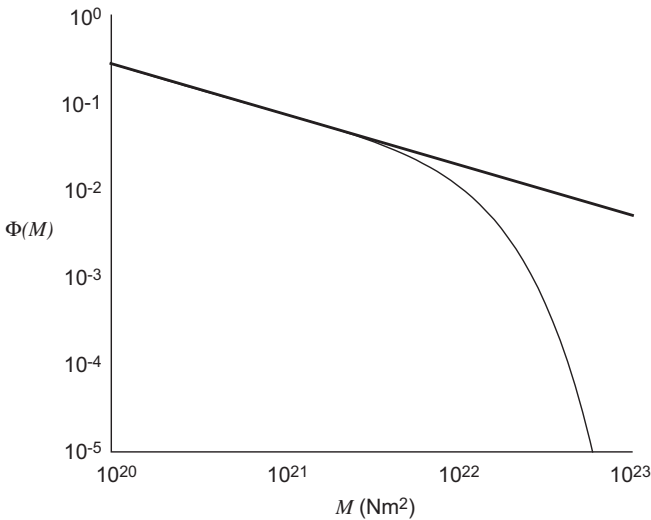


Figure 2.12 Comparison of complementary cumulative distribution functions for the unbounded Pareto distribution (heavy line) and the bounded gamma distribution (light line).

Of interest also is the overall occurrence rate of earthquakes in a particular region: i.e., the a -value in the G-R relation. The occurrence rate (α) for earthquakes of seismic moment $\geq M_0$ can be determined from the distribution parameters above and if the seismic moment release rate \dot{M}_s is known. The expression below, for example, gives the occurrence rate for the gamma distribution (Eqn [2.6]) (Kagan, 2002c):

$$\alpha(M \geq M_0) = \xi_g^{-1} \left[\frac{1 - \beta}{\Gamma(2 - \beta)} \right] \frac{\dot{M}_s}{\beta M_0^\beta M_c^{1-\beta}}, \quad [2.7]$$

where ξ_g is a correction coefficient. Initially, it was thought that α is proportional to the relative velocity of the plates across the boundary zone (Bird & Kagan, 2004; Kreemer, Holt, & Haines, 2002). However, a more recent study (Bird, Kagan, Jackson, Schoenberg, & Werner, 2009) using a nonparametric statistical test falsifies the hypothesis of a linear relation. Instead, subduction earthquake occurrence rates normalized with respect to relative plate velocity rates appear to increase with increasing plate velocity. Once the occurrence rate α associated with M_0 is known, the scale parameter for the distribution of inter-event times (discussed in the next section) can be linked to α (Corral, 2004b).

Earthquakes on a single fault or fault segment are thought by some to follow a characteristic distribution, in which the rate of the largest earthquake that spans an entire fault or fault segment is distinct from the rates of smaller earthquakes that follow a truncated G-R relation (Fig. 2.13(a)). Thus, in this conceptual framework, there are two populations of earthquakes: the characteristic earthquake defined by its magnitude and occurrence rate (m_c and α_c , respectively) and regular earthquakes that follow a G-R relation truncated at the magnitude of the characteristic earthquake's largest aftershock (Wessonsky, 1994). The characteristic distribution can also be defined as a truncation of the Pareto distribution in the cumulative form (Kagan, 1993, 2002a) as described above and shown in Fig. 2.13(b). In this case, the two populations are not distinct; rather, the characteristic earthquake is a density spike as part of the regular earthquake distribution. As indicated by Kagan (1993, 1996), the characteristic distribution is difficult to test, owing to the general subjective nature of defining characteristic earthquakes and the fact that the fault segments that define characteristic earthquakes are frequently defined by the earthquakes themselves (introducing an obvious bias).

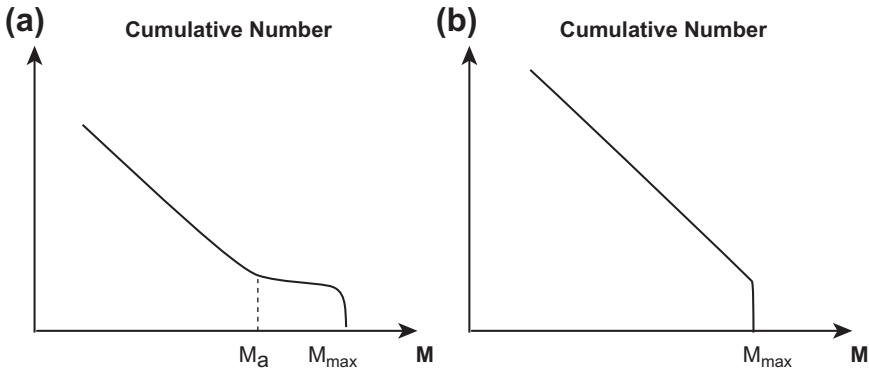


Figure 2.13 Two different forms of the characteristic size distribution for earthquakes. (a) Distribution of two distinct populations of earthquakes: regular earthquakes that follow a G-R distribution up to $M = M_a$ and the characteristic earthquake $M = M_{max}$. (b) Truncation of the G-R distribution at $M = M_{max}$.

However, theoretical and numerical fault mechanic studies have yielded results that mimic characteristic earthquakes as described in empirical studies (paleoseismic and historic seismicity patterns). Rice (1993) indicates that the generic result of rupture on a smooth fault using rate- and state-dependent friction is limit-cycles of repeated large earthquakes that span the entire fault. The study of Ben-Zion and Rice (1997) suggests that strong fault zone heterogeneities (geometrical and/or frictional parameters) are necessary to generate a broad distribution of earthquake sizes, consistent with the modified Pareto distributions. Further results from simulations of heterogeneous faults indicate an evolutionary cycle of power-law type earthquake size distributions punctuated by system-wide earthquakes (Ben-Zion, Eneva, & Liu, 2003; Dahmen, Ertas, & Ben-Zion, 1998).

An intriguing consequence of the nonlinear nature of the constitutive law for fault friction combined with fault heterogeneities and rupture dynamics is spontaneous mode switching between G-R and characteristic behaviors (Ben-Zion, 2008; Hillers, Carlson, & Archuleta, 2009; Zöller, Holschneider, & Ben-Zion, 2004). It has been suggested that a supercritical, branching fault system exhibiting characteristic behavior is not likely to persist for very long (Al-Kindy & Main, 2003; Vere-Jones, 1976). The aforementioned theoretical studies indicate that earthquake size distributions on a single fault are dependent on the degree of fault zone heterogeneity, with smooth faults necessary to generate characteristic distributions. For the case of sufficient heterogeneity, the suggestion that size distribution may be

nonstationary presents significant complications in interpreting the historical earthquake catalog and paleoseismic record.

Heterogeneities and branching structures in fault geometry may be key to understanding the size distributions of earthquakes in a region or zone near the fault (G-R behavior) versus distributions on a single smooth fault segment (characteristic behavior). Consideration of errors in earthquake location and of the mapped fault trace justifies using a wide zone (e.g., 100 km) to associate earthquakes with a particular plate-boundary fault (Bird & Kagan, 2004). Parsons and Geist (2009) indicate that G-R behavior persists even for a narrow region (e.g., ± 5 km) along the fault, if a long enough catalog is available: i.e., a tradeoff exists between the fault zone width and catalog duration as to when G-R behavior becomes apparent. Even in a narrow zone, such as ± 5 km along the fault trace, there are minor subsidiary faults that branch off or are subparallel to the main fault. It is possible that there is an inherent fractal nature of faults (of the fault surface and of branching fault lengths) that is behind the power-law nature of fault zone size distributions (Aviles, Scholz, & Boatwright, 1987; Clark, Cox, & Laslett, 1999; Fukao & Furumoto, 1985; Kagan, 1993; Molchan & Kronrod, 2009; Okubo & Aki, 1987; Ouillon, Castaing, & Sornette, 1996; Power & Tullis, 1991), though Kagan (1996) indicates a power-law distribution of fault sizes and characteristic earthquakes on those faults do not necessarily correspond to the observed earthquake statistics.

Though much less information is available regarding the size distribution of submarine landslides, owing to the lack of an instrumental record of occurrence, several studies indicate the existence of a Pareto size distribution for landslides, analogous to the standard G-R relation for earthquakes. ten Brink, Geist, and Andrews (2006) demonstrated that the distribution of submarine landslides north of Puerto Rico follow a Pareto distribution with an exponent (β) similar to that found for rock falls on land (Dussauge, Grasso, & Helmstetter, 2003; Guzzetti, Malamud, Turcotte, & Reichenbach, 2002; Malamud, Turcotte, Guzzetti, & Reichenbach, 2004; Stark & Hovius, 2001). Unlike earthquakes, the value of β varies significantly for landslides (e.g., comparison of the Storegga, Puerto Rico, and western Atlantic landslide regions: $\beta = 0.44, 0.64,$ and 1.3 respectively), indicating that the failure process and composition significantly affect scaling (ten Brink et al., 2006; Chaytor, ten Brink, Solow, & Andrews, 2009; Malamud et al., 2004). Chaytor et al. (2009) indicates that landslides along the western Atlantic continental slope are best fit by a lognormal distribution, but this may be due to a censoring effect where an underlying Pareto distribution is

modified by the conditional probability of observing landslides in shipboard-acquired bathymetric data. Stark and Hovius (2001) examined landslide areas over several orders of magnitude for on-land data, and proposed a double Pareto distribution that includes the effects of censoring:

$$\varphi(A) = \frac{\alpha}{A_c(1 - \Phi(A_{\min}))} \left\{ \frac{[1 + (A_{\max}/A_c)^{-\beta}]^{\alpha/\beta}}{[1 + (A/A_c)^{-\beta}]^{1+\alpha/\beta}} \right\} (A/A_c)^{-\beta-1}, \quad [2.8]$$

where A_{\min} and A_{\max} are the observed minimum and maximum landslide areas and A_c is the crossover scale that separates the actual negative-exponent (β) power-law relationship of landslide area (cf., Eqn [2.5]) from a positive-exponent (α) power-law that models the censoring effect (term in braces in Eqn [2.8]). ten Brink, Barkan, Andrews, and Chaytor (2009b) maintain, however, that submarine landslides are physically distinct from subaerial landslides, in which the lognormal and Pareto size distributions, respectively, reflect differences in slope morphology, with large subaerial landslides more related to a cascade process over a wide distribution of slopes, whereas large submarine landslides are the result of simultaneous failure over a uniform slope.

In examining the physical mechanisms that give rise to a power-law relationship, Hergarten and Neugebauer (1998) indicate that a state variable, in addition to slope gradient, is necessary for landslides to follow a power-law size distribution. This is generally termed a time-weakening effect (Densmore, Ellis, & Anderson, 1998; Hergarten, 2003), in which the probability of failure increases with waiting time after the last event at a particular source location. Examples of time-weakening effects include strain softening, creep, and redistribution of pore pressures following earthquakes (Biscontin & Pestana, 2006; Biscontin, Pestana, & Nadim, 2004). Dugan and Flemings (2000) also described a process of lateral pressure equilibration over time for submarine fans, with a gradual increase in the likelihood for failure.

3.2 Source Inter-event Time Statistics

In the same way as tsunami sizes are dependent on the size distribution of their sources, the temporal occurrence of tsunamis is also dependent on the temporal occurrence of the sources. The least astonishing hypothesis for a temporal description of source occurrence is the Poisson process, in which the time intervals between consecutive sources (i.e., the inter-event times)

are mutually independent (Feller, 1968). For earthquakes, it is commonly assumed that the occurrence rate for spontaneous events is stationary, owing to the constancy of long-term fault slip rates. For landslides, however, there has been considerable discussion as to the dependence of landslide rates on climatic changes and glacial cycles (e.g., Lee, 2009). More complex inter-event distributions that are alternatives to the Poisson null hypothesis can be subdivided into quasiperiodic distributions and cluster distributions as described below and in Fig. 2.14, primarily with regard to earthquake occurrence.

Quasiperiodic distributions describe temporal occurrence patterns that are dependent on the time since the last earthquake (τ), with a generally increasing hazard rate with respect to increasing τ . Commonly invoked quasiperiodic distribution models include Weibull, lognormal, and Brownian passage time (Matthews, Ellsworth, & Reasenberg, 2002; Utsu, 1984). Much like characteristic size distribution, these inter-event distributions are most often applied to individual faults. The seismic gap hypothesis combines the idea of characteristic-size earthquakes with quasiperiodic occurrence (McCann, Nishenko, Sykes, & Krause, 1979; Nishenko, 1991; Nishenko & Buland, 1987), though several statistical tests have refuted this hypothesis (Kagan & Jackson, 1991a, 1995; Rong, Jackson, & Kagan, 2003). Still, there does seem to be individual cases where a time-dependent, quasiperiodic distribution is the most appropriate model for earthquakes on a given fault (Parsons, 2008a) that Ben-Zion (1996) ascribes to a narrow range of size

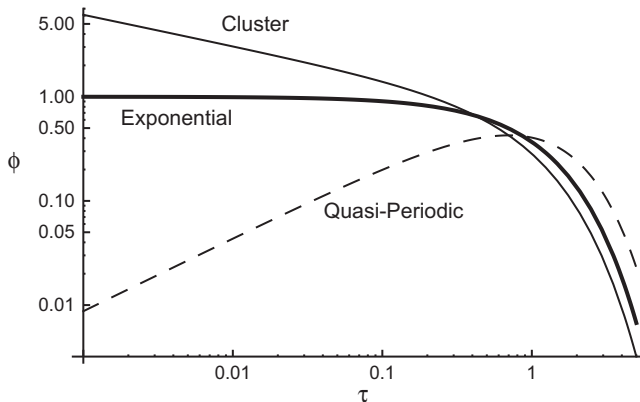


Figure 2.14 Examples of cluster (light solid line) and quasi-periodic (dashed line) distributions of inter-event times, in relation to an exponential distribution associated with a stationary Poisson process (heavy solid line). Log-log plot of probability density functions is shown.

scales for fault zone heterogeneities. Fitting these distributions to uncertain paleoseismic data is discussed by Ogata (1999) and Parsons (2008b).

Cluster distributions appear to best fit instrumental earthquake catalogs, primarily in the context of foreshock–main shock–aftershock sequences. The modified Omori law classically describes aftershock sequences (cf., Utsu, 2003) as well as triggered earthquakes (e.g., Parsons, 2002):

$$n(t) = \frac{K}{(t + c)^p}, \quad [2.9]$$

where $n(t)$ is the number of aftershocks over a particular time interval at time t after the main shock and K , c , and p are constants. Various conceptual statistical models such as the epidemic-type aftershock sequence (ETAS, discussed further in Section 4.2) (e.g., Helmstetter & Sornette, 2002; Ogata, 1988; Saichev & Sornette, 2007) and gamma distributions (Corral, 2004a, 2005) also have been used to describe the clustering process over various time scales.

Long-term clustering beyond foreshock–main shock–aftershock sequences is more difficult to detect. Spontaneous earthquakes or main shocks not associated with a triggered sequence are thought to follow a Poisson process as originally described by Gardner and Knopoff (1974). Since then, several studies have suggested the existence of long-term dependency in earthquake inter-event times from various causes (Kagan & Jackson, 1991b; Lennartz, Bunde, & Turcotte, 2011; Ogata & Abe, 1991; Selva & Marzocchi, 2005), although the results are often influenced by the choice and application of the declustering algorithms used to filter out dependent or triggered events (Hainzl, Scherbaum, & Beauval, 2006; Wang, Jackson, & Zhuang, 2010a, 2010b; Zhuang et al., 2008).

3.3 Tsunami Size Statistics

Evidence of scaling between earthquake magnitude and tsunami size (Section 2) suggests that the distribution of tsunami sizes should be similar in form to that of earthquakes (i.e., a modified Pareto distribution as described in Section 3.2). It is unclear, however, how much propagation and site response may affect the form and parameters of the size distribution. The focus in this section is determining the size distribution at a particular tide-gauge location. Although it is tempting to also analyze the size distribution for the global catalog of tsunamis, this catalog is likely strongly heterogeneous in terms of sizes, owing to site effects. This problem is not a factor, however, in analyzing inter-event times for the

global catalog (discussed in Section 3.4) since tsunami origin times at the source are analyzed.

Recent studies (Burroughs & Tebbens, 2005; Geist & Parsons, 2006; Geist et al., 2009b) suggest that the size distribution of tsunamis at a point on the coast follows a Pareto distribution, consistent with the size distribution of earthquakes (and many landslides). Like earthquakes, the size distribution for the largest tsunamis decays much faster than the power-law exponent (β), either due to under-sampling at large amplitudes (Burroughs & Tebbens, 2001) or because of increasing energy dissipation during propagation at large amplitudes (Geist, Lynett, & Chaytor, 2009a; Korycansky & Lynett, 2005). Several modified Pareto distributions, such as the gamma distribution (Eqn [2.6]), can be considered for tsunami maximum amplitudes (A), though a truncated density distribution (equivalent to the truncated G-R distribution of Kagan (2002a) is considered by Burroughs and Tebbens (2001, 2005):

$$\varphi(A) = \frac{\beta A_t^\beta A_x^\beta}{(A_x^\beta - A_t^\beta) A^{(1+\beta)}}, \quad \text{for } A_t \leq A \leq A_x, \quad [2.10]$$

where A_x is the largest observed amplitude.

Many of the same issues that need to be addressed in parameter estimation for earthquake size distributions, such as catalog completeness, long-term rate changes, and non-Gaussian residuals, also apply to tsunamis. In analyzing tsunami catalogs one has to separate eyewitness observations, which have obvious censoring problems, from various instrumental records (tide gauges and bottom pressure recorders). These subcatalogs have been analyzed separately by Geist and Parsons (2006) and Geist *et al.* (2009b) in the case of the Acapulco tide-gauge station and surrounding region. Kijko and Sellevoll (1989, 1992) developed statistical methods to combine subcatalogs with different thresholds in analyzing earthquake size distributions. Here we focus only on maximum amplitudes recorded at tide-gauge stations since these events have the longest catalog duration (e.g., in comparison to bottom pressure records) and are the most homogeneous (in comparison to eyewitness observations). Examination of low-amplitude, tide-gauge measurements of tsunamis reveals the predominance of entries equal to 0.1 m. This is interpreted as a default reading in which a tsunami is detected in the presence of ambient noise, but no specific maximum amplitude reading can be made, particularly for analog records that existed prior to the 1980s (Mofjeld, 2009). For tide-gauge sites with sufficient amplitude range

and number of recorded events, catalog completeness is, therefore, nominally >0.1 m since the mid-twentieth century. Catalog completeness is discussed further in Section 3.4 and in Geist and Parsons (2011).

By way of example, the single parameter estimation methods described by Kagan (2002a) for earthquake data are applied to tsunami data. While the Hill (1975) estimator can be used to estimate β in the simple Pareto distribution (Sornette, 2004), Kagan (2002a) indicates that estimating β for the truncated or tapered Pareto distribution involves solving the following maximum-likelihood estimate solution by iteration:

$$\frac{1}{\hat{\beta}} - \frac{\log(A_u/A_t)}{(A_u/A_t)^{\hat{\beta}} - 1} - \frac{1}{n} \sum_{i=1}^n \log \frac{A_i}{A_t} = 0, \quad [2.11]$$

where A_u is an upper amplitude limit greater than the assumed truncation (A_x) or corner amplitude (A_c) for the distribution. To estimate the corner value of the tapered Pareto distribution, Kagan and Schoenberg (2001) derived the following closed form expression using the method of moments, subject to a bias correction they describe:

$$\hat{A}_c = \frac{1}{2[A_t\beta + (1-\beta)\bar{A}]} \sum_{i=1}^n A_i^2/n - A_t^2, \quad [2.12]$$

where \bar{A} is the sample mean Kagan (2002a) also describes a two-parameter estimation technique to jointly determine β and corner moment (in the case of earthquakes). The effect of non-Gaussian distributed errors on parameter estimation techniques has recently been discussed by Leonard *et al.* (2001) and Greenhough and Main (2008) for earthquakes and other natural phenomena. In particular, the Gaussian assumption, such as used for example by Burroughs and Tebbens (2005), may systematically overestimate the errors for small amplitudes in the distribution.

Using Eqns [2.11] and [2.12] for the tapered Pareto distribution, tsunami size distributions are determined for nine Pacific tide-gauge stations from 1904–2010. Two representative samples are shown in Fig. 2.15: Hilo, Hawai'i and Hachinohe, Japan, the latter also examined by Burroughs and Tebbens (2005). Results calculated here in combination with those of Burroughs and Tebbens (2005) indicate differences in β that appear to be significant and range between 0.49 (Hilo) and 1.25 (Mera, Japan). Given that the size distribution exponent for subduction zone earthquakes has been shown to be approximately constant (Bird & Kagan, 2004; Kagan, 1999, 2002a, 2002c), differences in β for tsunamis may therefore reflect local and regional site conditions affecting the maximum amplitude.

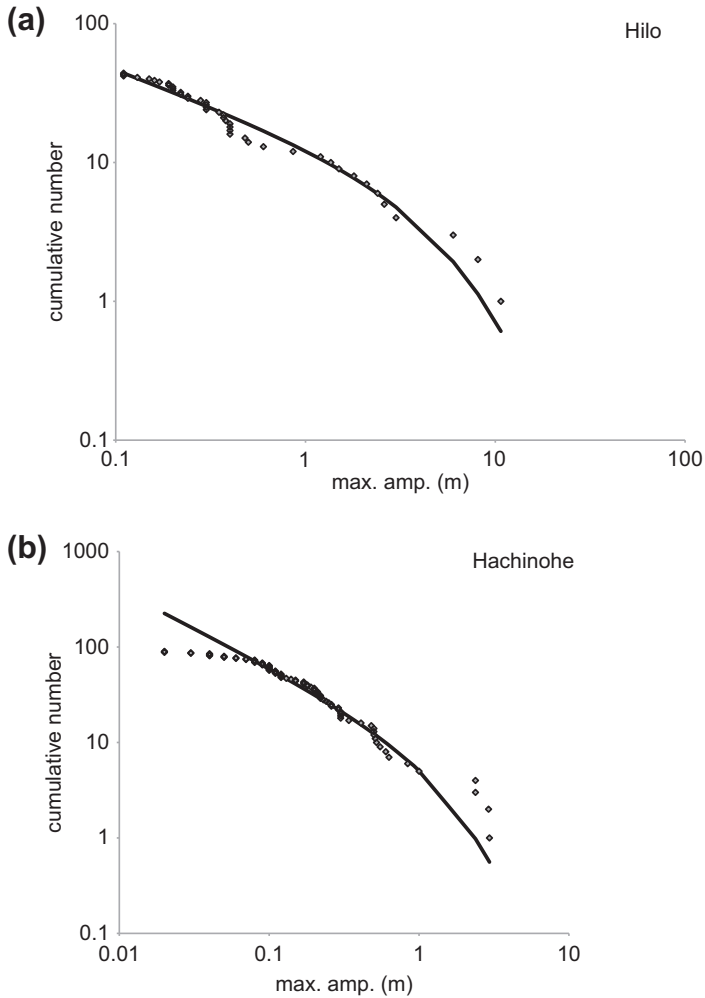


Figure 2.15 Size distribution of tsunami amplitudes (1904–2010) from two locations: (a) Hilo, Hawaii and (b) Hachinohe, Japan. Solid line represents a tapered Pareto distribution with maximum-likelihood parameter estimates.

As for earthquakes, the activity rate α for tsunamis can be determined based on the parameters of the size distribution (cf., Eqn [2.7]) or jointly with the size distribution parameters using tsunami frequency (year^{-1}) bins (Burroughs & Tebbens, 2005). Cumulative number plots as a function of historical time (e.g., Fig. 2.16) often suggest intermittent changes in the activity rate. At the beginning of the catalog shown in Fig. 2.16, the gradual increase in the rate of tsunami events being reported is linked to an increase

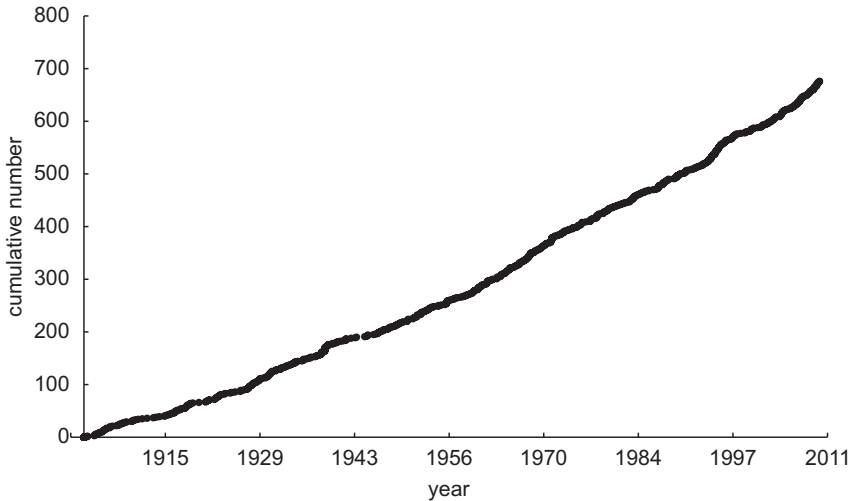


Figure 2.16 Cumulative number of all global tsunamis from 1904 to 2010.

in the number of tide-gauge stations worldwide. Detection thresholds of tsunami size and inter-event times are shown in Fig. 2.17. After an increase in the number of reporting stations in the years following the 1946 Aleutian tsunami, the rate of tsunamis of decimeter size or greater became nominally constant by the late 1950s. The rate of significant tsunamis greater than 1 m, however, appears to be stable since the beginning of the twentieth century (Geist & Parsons, 2011). Seismicity rate changes around 1922 and 1948, that are ascribed to differences in instrumentation and reporting procedures by Pérez and Scholz (1984) and to long-range correlations by Ogata and Abe (1991), are difficult to detect in cumulative number distribution (Fig. 2.16).

One of the more noticeable apparent rate changes occurs in the mid-1990s, when the rate of global tsunamis increased for a few years (Satake & Imamura, 1995). Various statistical methods have been developed for earthquake catalogs to determine whether similar changes are caused by random fluctuations associated with a stationary Poisson process, catalog heterogeneity (e.g., Pérez & Scholz, 1984), short-range dependence such as aftershock sequences, or long-range dependence. For example, Matthews and Reasenber (1988) developed a statistical test to distinguish periods of quiescence relative to a stationary null hypothesis. However, because this statistic tests the background rate of spontaneous earthquakes, it is necessary to decluster the catalog to remove aftershock sequences. For

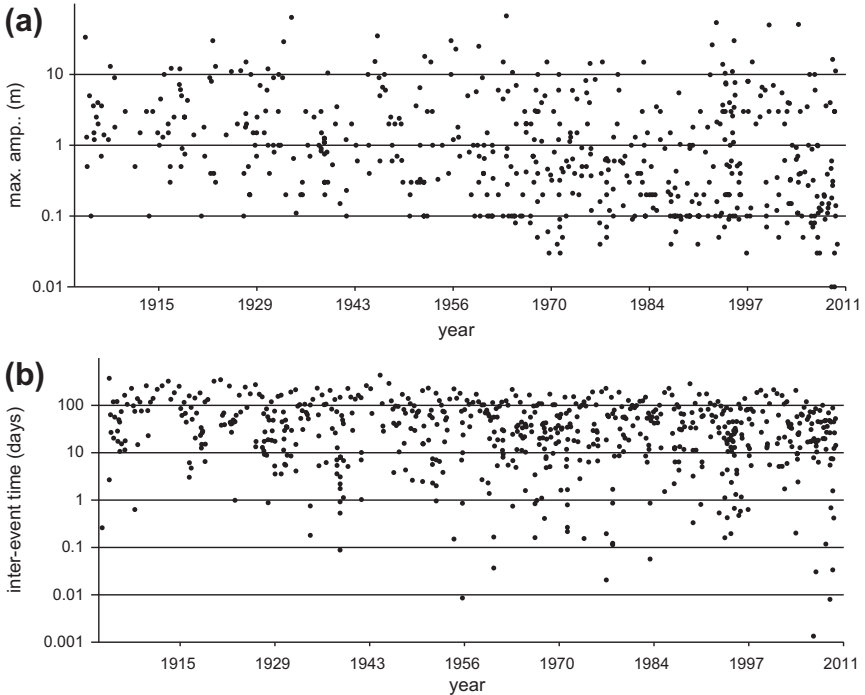


Figure 2.17 Detection limits over time: (a) maximum amplitude and (b) inter-event time.

the tsunami catalog, it is desirable to retain any events caused by aftershocks, triggered earthquakes, or landslides to first see if the observed rate changes are consistent with a Poisson process (Geist & Parsons, 2011). Marsan and Nalbant (2005) described different methods to test earthquake rate changes without declustering the catalog. Matthews and Reasenberg (1988) also described kernel estimation methods that can be used on the raw catalog to visually detect rate changes. Shown in Fig. 2.18 are annual counts of tsunamis >1 m along with a kernel density estimate of the data (solid line). A biweight kernel is used in this case, in which the bandwidth is chosen to minimize the mean integrated square error (Silverman, 1998). The result is a smooth nonparametric estimation of the occurrence rate and indicates that the mid-1990s is the most anomalous over the last century (see also Geist & Parsons, 2011). Finally, Ogata and Abe (1991) provided methods to determine the presence of long-range dependence in catalog data and argued that for events that do exhibit long-range dependence, it is difficult to completely decluster dependent events in the catalog.

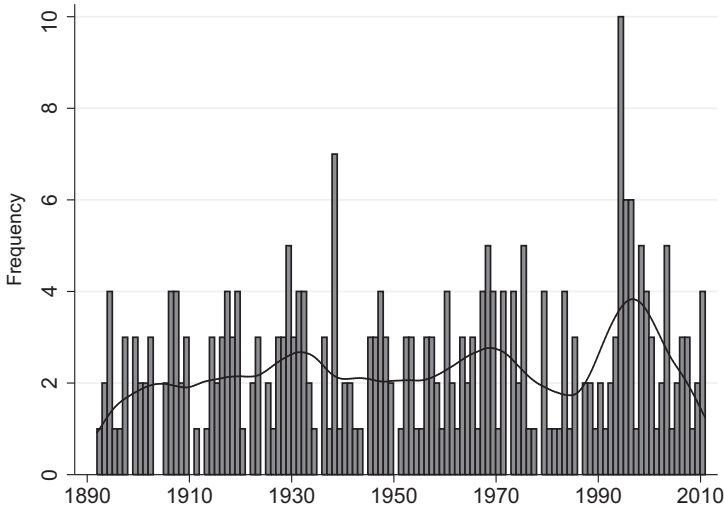


Figure 2.18 Histogram of tsunami event numbers since 1890. Density of global tsunami events determined from kernel estimation techniques (solid curve). See Geist and Parsons (2011).

3.4 Tsunami Inter-event Time Statistics

The distribution of tsunami inter-event times can shed some light on the fundamental features of tsunami temporal occurrence. In studies by Geist and Parsons (2008, 2011), the inter-event distribution is determined for both global tsunami sources and tsunami events at a specific location (Hilo, Hawai'i). Their findings indicate that there is significantly more temporal clustering compared to a Poisson process. For example, Fig. 2.19 shows the empirical density distribution (circles) for global tsunami sources that generate maximum run-up > 1 m. The dashed line in Fig. 2.19 shows the exponential distribution expected from a Poisson process. There are several temporal clustering models that can provide a better fit to the empirical distribution than the exponential model, including the gamma cluster model (solid line in Fig. 2.19) (Corral, 2004b), a probability distribution derived from the ETAS model (Section 4.2) (Saichev & Sornette, 2007), and the modified Omori law (Geist & Parsons, 2008).

Determination of the empirical inter-event distribution at a particular recording station is more difficult, owing to fewer events compared to the global tsunami source catalog and to the problem of detecting events spaced close in time. As an example, the empirical distribution of tsunamis at the Hilo, Hawai'i tide-gauge station is presented in Geist and Parsons (2008). Accurate empirical measurement of short inter-event times depends on the

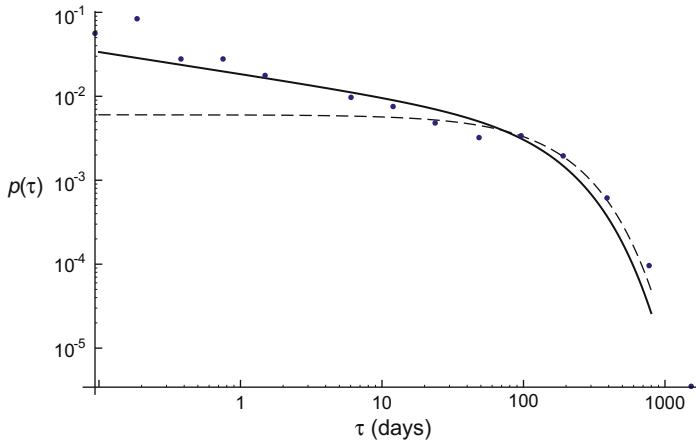


Figure 2.19 Density distribution of inter-event times for tsunami sources that generate maximum tsunami run-ups >1 m.

Modified from Geist and Parsons (2011).

detection of events near or within the coda of a preceding event. A similar issue has been described for earthquake occurrence probability models involving small aftershocks occurring close in time relative to the main shock. The c -value in the modified Omori formula (Eqn [2.9]) represents a saturation of short inter-event times, owing to a detection limit, although the conventional use of $c > 0$ implies that the singularity in aftershock rate occurs before the main shock, which is unphysical (Kagan & Houston, 2005). Kagan (1991, 2005) presents a probability model that explicitly includes the coda duration. Overall, the detectable presence of temporal clustering for tsunami occurrence introduces some complexity in analyzing the tsunami catalog compared to a simple stationary Poisson process. The hazard rate function associated with a clustered distribution indicates that there is an increased likelihood of tsunami occurrence shortly after each event that decreases with time compared to a Poisson process, whose hazard rate function is constant with time (Corral, 2005; Geist & Parsons, 2008).

A question not fully addressed in the Geist and Parsons (2008) study is whether triggering is a significant component of the clustering process. The physics of this will be discussed in the next section. In recent years, there have been several instances of significant tsunamis occurring close in time. For example, two tsunamis from the January 2009 $M_w = 7.6$ and $M_w = 7.4$ West Papua earthquakes are clearly distinguishable on local tide-gauge stations (Manokwari, Indonesia), spaced 2 h 50 min apart. In addition, separate

tsunamis from the October 2009 $M_w=7.7$ and $M_w=7.8$ Vanuatu earthquakes spaced 15 min apart are identifiable on bottom pressure sensors (Fig. 2.20). Before the deployment of bottom pressure sensors in the deep ocean, it was a difficult detection problem to distinguish two separate tsunamis occurring close in time and space on, for example, tide-gauge records. However, because the exponential decay of the tsunami coda is shorter on bottom pressure records than on tide-gauge records (cf., PT1), events occurring close in time and space are more likely to be detected. The difference in the detection capabilities of tsunami events in time is, therefore, likely to have an effect on parameter estimation for the cluster process, depending on the model. Figure 2.17(b) indicates that the minimum detection threshold for inter-event times has been decreasing over the last century.

Recently Geist and Parsons (2011) identified “mini-clusters” of tsunami sources that are likely to consist of triggered events. These clusters are identified as having both anomalously short inter-event times and are sourced within the same geographic region as identified in the tsunami catalog. Tsunami mini-clusters consist of only 2–4 events, in contrast to earthquake clusters that comprise a protracted sequence of events. The clusters themselves, along with spontaneous tsunami events, are characteristic of a Poisson cluster process (Bordenave & Torrisi, 2007; Kagan & Jackson, 2011; Kagan & Knopoff, 1987; Ogata, 1998). Random temporal grouping of geographically distinct mini-clusters according to a Poisson cluster process is a likely explanation of the rate changes observed in Fig. 2.18 (Geist & Parsons, 2011).

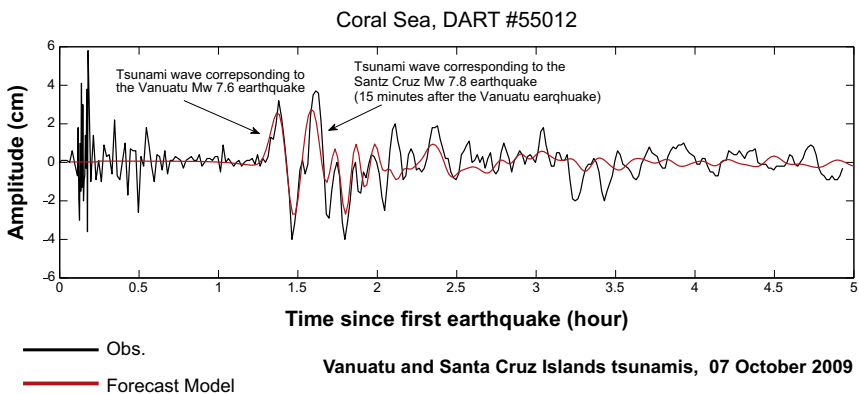


Figure 2.20 Examples of tsunami events occurring close in time as recorded by bottom pressure recording stations. (Courtesy, NOAA/PMEL).



4. INTER-EVENT TRIGGERING

There is likely a physical cause for tsunami sources occurring close in time and space, in which one source triggers subsequent sources. Inter-event triggering can be thought of as a stochastic branching process, where an earthquake may trigger other earthquakes, one of which may then trigger a landslide, etc. In this section, different conceptual models of triggering are reviewed, both for earthquake-to-earthquake and earthquake-to-landslide triggering (the most common triggering mechanisms), followed by a summary of empirical observations and statistical triggering models derived from earthquake studies.

4.1 Earthquake-to-earthquake Triggering

Near-field triggering of earthquakes is typically governed by the transfer of static stress from one fault to another or along the same fault, from one segment to another (see [Harris, 1998](#) and references therein). The primary physical variable is the Coulomb failure stress (ΔC_f) that includes normal and shear stress components resolved on the receiver fault:

$$\Delta C_f = |\Delta\tau| + \mu(\Delta\sigma_n + \Delta p), \quad [2.13]$$

where $\Delta\tau$ and $\Delta\sigma_n$ are the changes in shear and normal stress, respectively, μ is the static coefficient of friction, and Δp is the change in pore pressure along the fault. Numerous studies have shown an increase in the occurrence rate of earthquakes in regions of positive ΔC_f and an attendant decrease in earthquake occurrence in regions of negative ΔC_f (i.e., stress shadows) (e.g., [Reasenbergs & Simpson, 1992](#); [Stein, 1999](#)). More recently, [Hainzl, Zöller, and Wang \(2010\)](#) consider a distribution of receiver fault orientation and find that for such a distribution, stress shadows are attenuated. [Parsons, Ogata, Zhuang, and Geist \(2012\)](#) provide prospective and blind tests of the static stress change hypothesis for triggering and find that, although the existence of secondary triggered earthquakes (e.g., predicted by the ETAS branching model) obviates confirmation of static triggering, the hypothesis has significant predictive ability for large earthquakes ($M > 6$).

Dynamic friction described by rate-and-state equations provides an additional insight into the earthquake triggering process, in comparison to the static friction (μ) used in the Coulomb failure stress (Eqn [2.13]) ([Harris & Simpson, 1998](#)). Shear stress progressively increases with time along a fault owing to (remote) tectonic loading (proportional to the relative plate speed V)

and intermittently changes according to stress concentrations from ruptures on adjacent patches along a fault or on neighboring faults that might be nearby. This is summarized by Dieterich (1995):

$$\tau_1 = K_{12}D_{12} + K_T(Vt - D_1), \quad [2.14]$$

where subscript 1 is the receiver fault patch, subscript 2 is an antecedent fault patch (triggering earthquake) that has slipped amount D , K_{12} is the stiffness matrix describing the elastic interaction between fault patches, and K_T is the stiffness term for tectonic loading. The time-dependent breakdown in fault strength associated with a stress step from a previous earthquake in the rate-and-state formulation provides a physical explanation for temporal and spatial clustering of earthquakes along a fault. In general, spatial heterogeneity of slip appears to be a controlling factor in clustering statistics (Dieterich, 1995; Hainzl, Zöller, & Scherbaum, 2003). However, other physical mechanisms (e.g., involving damage mechanics or pore-fluid pressure) have also been proposed to explain earthquake clustering (Main, 2000a; Yamashita, 1999).

Recently, it has been proposed by a number of authors that dynamic triggering can occur by the passage of seismic waves. Examples of large-magnitude earthquakes that dynamically triggered subsequent events in the far-field include the $M=9.2$ Sumatra–Andaman earthquake as observed in Alaska (West, Sánchez, & McNutt, 2005) and the $M=7.9$ Denali earthquake as observed along the US west coast (Prejean et al., 2004). Because high stress amplitudes, relative to typical seismic waves, are necessary to trigger earthquakes under normal tectonic loading conditions (Dieterich, 2007), anomalous properties of the receiver fault are thought to be necessary for far-field, dynamic triggering to take place. Heightened pore pressures within the fault zone are the most common explanation of dynamic triggering (Brodsky, Roeloffs, Woodcock, Gall, & Manga, 2003; Dieterich, 2007).

Several recent studies have examined statistical evidence for inter-event triggering in the earthquake catalog. Parsons (2002) calculated the static stress change for 117 $M_s \geq 7.0$ global earthquakes and determined that 8% of the earthquakes in the CMT catalog are triggered and that 61% of those events occur in regions of stress increase. Globally, the triggered earthquakes follow the Omori law temporal decay that persists 7–11 years. Parsons and Velasco (2009) found that near the source, static stress change is the most likely triggering mechanism compared to dynamic triggering. Farther from the source, where small and micro-earthquakes are commonly triggered by

the passage of seismic waves (Velasco, Hernandez, Parsons, & Pankow, 2008), Parsons and Velasco (2011) found no temporal association of $M \geq 5$ earthquakes (i.e., of tsunamigenic magnitude) with seismic waves from $M \geq 7$ earthquakes. Most of the triggering effects for earthquakes of tsunamigenic magnitude appear to be related to static stress changes and are expected within a radius of approximately 1000 km from the primary event.

4.2 Earthquake-to-landslide triggering

Examination of a global tsunami catalog indicates that most tsunamigenic landslides are triggered by earthquakes, much like subaerial landslides in seismically active regions (Keefer, 1994). For non-seismically triggered landslides, very low tidal excursions are a common triggering mechanism in which the slide loses its hydraulic support and does not dewater rapidly. Other potential non-seismic sources include subaerial failures entering the water, particularly in fjords, typically triggered by changes in pore pressure or wave action at the base of a coastal cliff. Overall, landslide sources without a seismic trigger that generate significant tsunamis are quite rare.

The relationship between earthquakes and the initiation of landslides has traditionally been analyzed using the Newmark rigid block method (Newmark, 1965). This method relates permanent displacement of a surficial block on an inclined plane to earthquake shaking. The method has since been improved to include the dynamic response of the surficial layer (i.e., compliance) and multidirectional seismic displacements (Kayen & Ozaki, 2002; Ozaki, Takada, & Kayen, 2001). In addition to direct loading from the earthquake, changes in pore pressure from individual and successive seismic loading cycles are also thought to be important in understanding the seismic triggering mechanism of subaqueous landslides (Biscontin & Pestana, 2006; Biscontin et al., 2004; Kokusho, 1999; Stegmann, Strasser, Anselmetti, & Kopf, 2007; Stigall & Dugan, 2010). Movement along the basal slip plane has been considered analogous to rupture propagation on a fault by Martel (2004) and Viesca and Rice (2010); the latter study takes into account evolving permeability and elastic-plastic deformation during basal slip.

To determine the area in which landslides are likely to be triggered relative to earthquake locations, ten Brink, Lee, Geist, and Twichell (2009a) compared analytic slope-stability methods with results from empirical relationships for subaerial landslides. For the former method (e.g., Lee, Locat, Dartnell, Minasian, & Wong, 2000), the maximum distance for which landslides can be triggered depends on the magnitude, seafloor slope, and the

assumed attenuation relationship to determine the peak spectral acceleration. For the latter method, a maximum liquefaction distance relative to the earthquake location is defined by Ambraseys (1988), whereas as a maximum total area of landslide failure is defined by Keefer (1984) and Rodriguez, Bommer, and Chandler (1999). ten Brink et al. (2009a) noted that the slope-stability method results in slightly smaller distance-to-failure and total failure areas than the empirical relationships, although both methods are consistent with the triggering of the 1929 Grand Banks tsunamigenic landslide by a $M_s = 7.2$ earthquake located at the steep upper slope of continental margin (Bent, 1995). In a later study, ten Brink et al. (2009b) drew a distinction between triggering of submarine and subaerial landslides according to their size distributions, generally preferring the slope-stability method.

4.3 Generalized Branching Process

Branching models have frequently been employed to describe earthquake occurrence. Each spontaneous event produces a random number of dependent events (“children”), each of which produces their own children etc. In its simplest form, the probability distribution for producing a certain number of children remains the same for the entire process. For application to aftershock sequences and triggered earthquakes, extinction occurs after a finite time and finite number of events. It should be emphasized, however, that in this model, triggered events can produce their own sequence of triggered events (i.e., secondary or indirect triggering). These events present difficulties in applying static stress change theory to small earthquakes (Parsons, Ogata, Zhuang, & Geist, 2012).

Perhaps the most common earthquake branching model is the ETAS model (Ogata, 1988). An alternative branching model, termed as the branching aftershock (BASS) model, has recently been proposed by Turcotte, Holliday, and Rundle (2007). Results from both models are consistent with the Omori law (Eqn [2.9]) for aftershock numbers and the G-R distribution of aftershock sizes. In its original form, the ETAS model describes the statistical characteristics of triggered events in terms of their temporal occurrence and magnitude, although Ogata and Zhuang (2006) extend the ETAS model to also describe the spatial occurrence of triggered earthquakes. The branching parameter n in ETAS is defined as the mean number of first-generation events triggered by an earthquake in the sequence (Helmstetter & Sornette, 2002). If $n < 1$ (subcritical regime), the ETAS model is consistent with Omori-like decay of aftershock numbers.

Saichev and Sornette (2007) also derived the inter-event time (τ) distribution corresponding to the ETAS model:

$$f(x) = \left[\frac{n\varepsilon^\theta}{x^{1+\theta}} + \left(1 - n + \frac{n\varepsilon^\theta}{x^\theta} \right)^2 \right] \varphi(x, \varepsilon), \quad [2.15]$$

where c and θ are constants in the Omori law, $x = \lambda\tau$, $\varepsilon = \lambda c$, and $\varphi(x, \varepsilon)$ is a universal scaling function. In their analysis of different earthquake catalogs, Saichev and Sornette (2007) estimated that the branching ratio is approximately $n \approx 0.9$.

In terms of magnitudes, the triggered earthquakes do not always have to be smaller than the master event, i.e., in the case of foreshocks. Kagan (2010) considers separate branching models for event magnitudes and the temporal occurrence of events. In contrast to the temporal branching model, the magnitude branching model is supercritical, resulting in power-law like behavior (i.e., G-R). Moreover, Kagan (2010) demonstrates that the negative binomial distribution of earthquake counts in large time and space windows is a consequence of this branching process. Interestingly, the parameter that characterizes clustering in the negative binomial distribution depends on the corner magnitude (M_c) of the size distribution (cf., Eqn [2.6]).

Earthquake branching models can be modified to describe tsunami occurrence (Fig. 2.21). In this case, a subset of the earthquake catalog is used

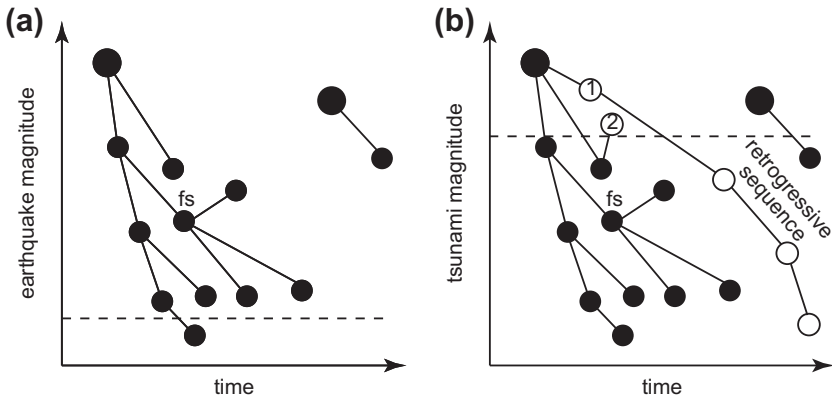
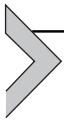


Figure 2.21 Schematic diagram of temporal branching for (a) earthquakes and (b) tsunamis of different magnitudes (vertical axis). Large circles represent spontaneous events. Dashed line indicates ground motion and water level detection levels, respectively. fs: foreshock succeeded by the earthquake of larger magnitude. Landslide events 1 and 2 are discussed in the text. After Kagan (2010).

in which events meet minimum criteria for tsunamigenesis (located at or near the ocean, above a certain magnitude to generate a detectable tsunami, etc.). An additional modification includes the fact that children of spontaneous tsunamigenic earthquake may include landslides (shown as open circles in Fig. 2.21). Spontaneous tsunamigenic landslides can be treated as “immigrants” in the branching process, but are unlikely to generate additional triggered events. Geist and Parsons (2008) indicate that the inter-event distribution (Eqn [2.15]) associated with the ETAS model is consistent with the observed inter-event times, although the branching parameter is much smaller ($n \approx 0.1$) than for complete earthquake catalogs at sub-tsunamigenic magnitude thresholds. This is likely due to a high detection threshold relative to the number of triggered events that actually occur (indicated by the dashed lines in Fig. 2.21). In the example shown in Fig. 2.21, only two landslide tsunami sources are detected by water-level measurements. One landslide event (labeled 1) is part of a retrogressive sequence (failures progressively occur upslope), only one of which generates a detectable tsunami. The other landslide (labeled 2) appears to be a spontaneous event, because the triggering earthquake is not detected by tsunami measurements.



5. DISCUSSION

An examination of how tsunami run-up and amplitude scale with earthquake source parameters indicates that the most robust scaling occurs with coseismic slip and seismic moment. Even with these parameters, however, there is significant predictive uncertainty, with the coefficient of determination (R^2) ranging between 0.4 and 0.6. In scaling local tsunami run-up with slip and seismic moment, certainly some of the uncertainty is caused by nearshore site effects. In examining far-field scaling, however, single-station scaling plots (Fig. 2.10) reveal similar ranges of R^2 . This suggests that variations in geometric and kinematic source parameters, as well as propagation path effects, such as reflections and scattering, also contribute to the uncertainty in scaling relationships.

With regard to earthquake sources, the effect of variations in geometric parameters of earthquake rupture is discussed in Geist (1999), whereas a statistical description of variations in the kinematics of coseismic slip is discussed in PT1 (Geist, 2009). In addition to spatiotemporal complexities arising from earthquake rupture dynamics, deviations from seismic moment-based scaling relations may also be ascribed to tsunamis generated by

triggered submarine landslides, at least in the near-field. The temporal evolution of seafloor deformation associated with landslide dynamics, rather than the triggering mechanism per se, is key to determining the magnitude of the wave that is produced, for a given failed volume of material. The diversity and nonlinearity of rheologies that submarine mass movements exhibit result in a wide range of temporal behaviors ranging from creeping (subcritical Froude number) to fast moving with a Froude number approaching one. Yield stress is a key material parameter that dictates the temporal behavior and is incorporated into most mass movement rheologies (PT1). It should also be mentioned that hydroplaning can occur during debris flow dynamics that can greatly increase the downslope speed of movement. Hydroplaning helps explain a paradox associated with submarine landslides: while buoyancy significantly reduces the gravitational driving force for submarine landslides relative to their subaerial counterparts, many submarine landslides exhibit much longer runout distances (De Blasio, Ilstad, Elverhøi, Issler, & Harbitz, 2004; Harbitz et al., 2003; Locat & Lee, 2002). Thus, for the subset of the tsunami catalog that has a landslide component, there can be large variability in the efficiency of tsunami generation.

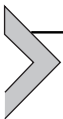
Because there is no routine instrumental recording of the occurrence of submarine landslides, the distribution of inter-event times for tsunami sources is limited to earthquakes. Although it has been shown that temporal clustering is evident for both global and regional earthquake catalogs (Corral, 2004b), it is unclear whether the subset of the earthquake catalog that meet the criteria for tsunamigenesis also exhibits clustering. Results from Geist and Parsons (2008; 2011) indicate that temporal clustering is observed for both tsunamigenic earthquakes and tsunami events recorded at a single tide-gauge station. Temporal clustering results in elevated rates of tsunami activity that persists for several years. Even though classical after-shock sequences are not readily apparent in tsunami catalogs, the spatial and temporal occurrence of tsunami clusters exhibit aftershock-like behavior in terms of triggering distance and temporal decay (cf., Parsons, 2002), even though the tsunami sources in a cluster are infrequently on the same fault.

With regard to the size distribution of tsunamis, it is less clear that tsunami events should follow the same distribution form as for earthquakes and landslides given the uncertainty in scaling relations between source size and tsunami size. Tsunami events recorded at single tide-gauge stations do appear to conform to a modified Pareto distribution, parameterized by a power-law exponent and corner amplitude. However, the power-law exponent appears to vary significantly from station to station, in contrast to

earthquake size distributions (Kagan, 1999). Landslide size distributions appear to have similar power-law exponents for a given composition of failed material, but the exponents can vary among different compositions (clastic, carbonate, etc.) (ten Brink et al., 2006).

Scaling of maximum, nearshore tsunami amplitude with earthquake magnitude, combined with a power-law like distribution of source sizes, implies that future observations of tsunami amplitude are likely to include amplitudes that are greater than those previously recorded, if the tsunami catalog is incomplete. For seismic ground motions, Yamada et al. (2009) showed that, although PGD is lognormally distributed for a given magnitude, the marginal distribution of PGD for an ensemble of earthquakes is more uniform than lognormal. This similarly applies to near-field tsunamis, as well as far-field tsunamis. In general, uncertainty in the amplitude–magnitude scaling is normally distributed (cf., Geist, 2002; Geist & Parsons, 2009 for the specific case of amplitude uncertainty caused by variations in slip distribution). Combining the probability of observing a certain amplitude for a given earthquake magnitude with the probability of an earthquake of a certain size, yields a non-Gaussian, Pareto distribution of tsunami sizes without a characteristic scale (e.g., Fig. 2.15).

Finally, it is worth noting that although tsunami sizes follow a power-law like distribution, they are not strictly a natural phenomenon that can be described as a self-organized critical (SOC) system. Rather, they are products of such systems in terms of earthquakes (Al-Kindy & Main, 2003; Main, 1995) and landslides (Hergarten & Neugebauer, 1998; Micallef, Berndt, Masson, & Stow, 2008). One aspect of SOC systems aside from the emergent power-law distribution of sizes is that they are characterized by a slowly driven dissipative process. This can be said for earthquakes, in which the driving force is the slow movement of tectonic plates and stress loading of the fault, and for submarine landslides, in which the driving force is the continual accumulation of sediment or coral growth. Thus, tsunamis are a response to SOC systems, rather than being an SOC itself.



6. SUMMARY

In this paper, three aspects of the phenomenology of tsunami events have been examined: scaling of tsunami waves with respect to their sources, statistics of tsunami sizes and inter-event times, and inter-event triggering. This material is intended to complement the material from PT1

(Geist, 2009) that examines the phenomenology of a single tsunami, from its generation to run-up at local and distant shores. In PT1, several hypotheses were offered that could be tested, and possibly falsified, with the acquisition of a handful of well-recorded future events. It is difficult to formulate similar hypotheses in this chapter, owing to the fact that better-constrained statistics requires addition of substantially more data to the tsunami catalog. Nevertheless, several general observations are apparent from past data as described below.

Local tsunami run-up and far-field tsunami amplitude appear to scale with seismic moment, although there is significant uncertainty in the correlation. Local tsunami run-up also appears to scale with mean slip for typical inter-plate thrust earthquakes. However, similar scaling is determined not to be significant at the 95% confidence level for tsunami earthquakes. The primary source of uncertainty in slip-run-up scaling is how the seismic inversions are formulated to determine slip. Both inter-plate thrust and tsunami earthquakes exhibit log-log scaling of seismic moment with respect to local run-up. For the largest magnitude earthquakes that generate transoceanic tsunamis, log-log scaling of seismic moment with respect to maximum tide-gauge amplitude is also significant. R^2 for local run-up and far-field amplitude range between approximately 0.4 and 0.6.

The size distribution of tsunami amplitudes at a particular recording station is similar in form to that of earthquakes (modified Pareto distribution), however, the power-law exponent appears to vary in contrast to earthquakes where it is more or less constant. Earthquake sizes most often follow the G-R distribution that is associated with a modified Pareto distribution. The fact that tsunami sizes scale with seismic moment suggests that tsunamis should follow the same distribution. The significant uncertainty in the scaling relationships, however, necessitates a quantitative appraisal of tsunami size distributions. Data from single tide-gauge stations that have recorded a sufficient number of events do indicate that maximum amplitudes are consistent with a modified Pareto distribution, parameterized by a power-law exponent and a corner amplitude. Both of these distribution parameters appear to vary significantly from station to station.

The inter-event time distribution for tsunamis is similar to that for earthquakes, in which temporal clustering of events is apparent. Both tsunamigenic earthquakes and tsunamis recorded at a single tide-gauge station exhibit significantly more short inter-event times relative to a stationary Poisson process (Geist & Parsons, 2008; 2011). There are a number of distribution models that fit the observations, including those that are also

used to model earthquake inter-event distributions (e.g., gamma and ETAS distributions). Although the distributions conform to Omori-like decay of earthquake aftershocks, classically defined aftershock sources for tsunamis are not readily apparent in the tsunami catalog. Rather, short sequences of triggered earthquakes on different faults appear to explain the temporal clustering of tsunami events (Geist & Parsons, 2011).

Temporal clustering of tsunami events can primarily be explained by earthquake-to-earthquake triggering, with occasional earthquake-to-landslide triggering also present. Earthquake-to-earthquake triggering occurs through a transfer of static stress from the fault that ruptured to a receiver fault. Dynamic earthquake triggering can also occur by the passage of seismic waves across a receiver fault, though for earthquakes of tsunamigenic magnitude, static triggering appears to be the dominant mechanism. Most tsunamigenic landslides listed in tsunami catalogs are triggered by earthquake shaking, through a loss of strength and a redistribution of pore pressure. A general branching model for triggering of tsunamigenic events that includes both earthquakes and landslides is proposed (Fig. 2.21), although the details of its parameterization and statistical testing await further development.

Finally, the overall objective of this study and PT1 is to place the unexpected behavior of tsunamis, for example, their unexpected size and frequency, in a statistical and probabilistic context. From a warning perspective, although one can estimate the size of a tsunami from the magnitude of the causative earthquake, there is significant uncertainty in this estimate. There are multiple factors for the cause of this uncertainty: variations in source parameters for a given seismic moment, triggered landslides, propagation path effects, and variations in site response. Short-term, time-dependent tsunami forecasts could be developed in the future based on the knowledge that there is a heightened likelihood of tsunamigenic events occurring close in time, compared to a stationary Poisson process, similar to the short-term earthquake probability effort (Gerstenberger, Wiemer, & Jones, 2004). From a hazard assessment perspective, the power-law like size distribution indicates that there is not a characteristic height at which tsunamis might occur at a particular location on the coast. This implies, most importantly, that past tsunamis are not likely to be reliable indicators of the largest tsunamis that might occur along a particular coast.

ACKNOWLEDGMENTS

The author would like to thank Tom Parsons and Alex Apotsos for interesting discussions and constructive reviews of this paper.

REFERENCES

- Abe, K. (1995). Estimate of tsunami run-up heights from earthquake magnitudes. In Y. Tsuchiya, & N. Shuto (Eds.), *Tsunami: Progress in Prediction, Disaster Prevention and Warning* (pp. 21–35). Dordrecht: Kluwer Academic Publishers.
- Al-Kindy, F. H., & Main, I. G. (2003). Testing self-organized criticality in the crust using entropy: a regionalized study of the CMT global earthquake catalogue. *Journal of Geophysical Research*, *108*. doi:10.1029/2002JB002230.
- Ambraseys, N. N. (1988). Engineering seismology. *Earthquake Engineering and Structural Dynamics*, *17*, 1–105.
- Apotos, A., Gelfenbaum, G., & Jaffe, B. (2012). Time-dependent onshore tsunami response. *Coastal Engineering*, *64*, 73–86.
- Atwater, B. F., & Hemphill-Haley, E. (1997). Recurrence intervals for great earthquakes of the past 3,500 years at northeastern Willapa Bay, Washington. Professional Paper Rep. 1576, p. 108, U.S. Geological Survey.
- Aviles, C. A., Scholz, C. H., & Boatwright, J. (1987). Fractal analysis applied to characteristic segments of the San Andreas fault. *Journal of Geophysical Research*, *92*, 331–344.
- Baptista, A. M., Priest, G. R., & Murty, T. S. (1993). Field survey of the 1992 Nicaragua tsunami. *Marine Geodesy*, *16*, 169–203.
- Bent, A. L. (1995). A complex double-couple source mechanism for the M_s 7.2 1929 Grand Banks earthquake. *Bulletin of the Seismological Society of America*, *85*, 1003–1020.
- Ben-Zion, Y., & Rice, J. R. (1997). Dynamic simulations of slip on a smooth fault in an elastic solid. *Journal of Geophysical Research*, *102*, 17,771–17,784.
- Ben-Zion, Y., Eneva, M., & Liu, Y. (2003). Large earthquake cycles and intermittent criticality on heterogeneous fault due to evolving stress and seismicity. *Journal of Geophysical Research*, *108*. doi:10.1029/2002JB002121.
- Ben-Zion, Y. (1996). Stress, slip, and earthquakes in models of complex single-fault systems incorporating brittle and creep deformations. *Journal of Geophysical Research*, *101*, 5677–5706.
- Ben-Zion, Y. (2008). Collective behavior of earthquakes and faults: continuum-discrete transitions, progressive evolutionary changes, and different dynamic regimes. *Reviews in Geophysics*, *46*. doi:10.1029/2008RG000260.
- Beresnev, I. A. (2003). Uncertainties in finite-fault slip inversions: to what extent to believe? (a critical review), *Bulletin of the Seismological Society of America*, *93*, 2445–2458.
- Bilek, S. L., & Lay, T. (1999). Rigidity variations with depth along interplate mega thrust faults in subduction zones. *Nature*, *400*, 443–446.
- Bird, P., & Kagan, Y. Y. (2004). Plate-tectonic analysis of shallow seismicity: apparent boundary width, beta-value, corner magnitude, coupled lithosphere thickness, and coupling in 7 tectonic settings. *Bulletin of the Seismological Society of America*, *94*, 2380–2399.
- Bird, P., Kagan, Y. Y., Jackson, D. D., Schoenberg, F. P., & Werner, M. J. (2009). Linear and nonlinear relations between relative plate velocity and seismicity. *Bulletin of the Seismological Society of America*, *99*, 3097–3113.
- Biscontin, G., & Pestana, J. M. (2006). Factors affecting seismic response of submarine slopes. *Natural Hazards and Earth System Sciences*, *6*, 97–107.
- Biscontin, G., Pestana, J. M., & Nadim, F. (2004). Seismic triggering of submarine slides in soft cohesive soil deposits. *Marine Geology*, *203*, 341–354.
- Boore, D. M. (1983). Stochastic simulation of high-frequency ground motions based on seismological models of the radiated spectra. *Bulletin of the Seismological Society of America*, *73*, 1865–1894.
- Bordenave, C., & Torrisi, G. L. (2007). Large deviations of Poisson cluster processes. *Stochastic Models*, *23*, 593–625.

- Bos, A. G., & Spakman, W. (2003). The resolving power of coseismic surface displacement data for fault slip distribution at depth. *Geophysical Research Letters*, *30*. doi:10.1029/2003GL017946.
- Brodsky, E. E., Roeloffs, E., Woodcock, D., Gall, I., & Manga, M. (2003). A mechanism for sustained groundwater pressure changes induced by distant earthquakes. *Journal of Geophysical Research*, *108*. doi:10.1029/2002JB002321.
- Brune, J. N. (1970). Tectonic stress and the spectra of seismic shear waves from earthquakes. *Journal of Geophysical Research*, *75*, 4997–5009.
- Burroughs, S. M., & Tebbens, S. F. (2001). Upper-truncated power laws in natural systems. *Pure and Applied Geophysics*, *158*, 741–757.
- Burroughs, S. M., & Tebbens, S. F. (2005). Power law scaling and probabilistic forecasting of tsunami run up heights. *Pure and Applied Geophysics*, *162*, 331–342.
- Byrne, D. E., Davis, D. M., & Sykes, L. R. (1988). Loci and maximum size of thrust earthquakes and the mechanics of the shallow region of subduction zones. *Tectonics*, *7*, 833–857.
- Cartwright, D. E., & Longuet-Higgins, M. S. (1956). The statistical distribution of the maxima of a random function. *Proceedings of the Royal Society of London A*, *237*, 212–232.
- Chaytor, J. D., ten Brink, U. S., Solow, A. R., & Andrews, B. D. (2009). Size distribution of submarine landslides along the U.S. Atlantic Margin. *Marine Geology* 16–27.
- Choi, B. H., Pelinovsky, E., Ryabov, I., & Hong, S. J. (2002). Distribution functions of tsunami wave heights. *Natural Hazards*, *25*, 1–21.
- Choi, B. H., Hong, S. J., & Pelinovsky, E. (2006). Distribution of runup heights of the December 26, 2004 tsunami in the Indian Ocean. *Geophysical Research Letters*, *33*. doi:10.1029/2006GL025867.
- Clark, R. M., Cox, S. J. D., & Laslett, G. M. (1999). Generalizations of power-law distributions applicable to sampled fault-trace lengths: model choice, parameter estimation and caveats. *Geophysical Journal International*, *136*, 357–372.
- Comer, R. P. (1980). Tsunami height and earthquake magnitude: Theoretical basis of an empirical relation. *Geophysical Research Letters*, *7*, 445–448.
- Corral, A. (2004a). Long-term clustering, scaling, and universality in the temporal occurrence of earthquakes. *Physical Review Letters*, *92*. doi:10.1103/PhysRevLett.1192.108501.
- Corral, A. (2004b). Universal local versus unified global scaling laws in the statistics of seismicity. *Physica A*, *340*, 590–597.
- Corral, A. (2005). Time-decreasing hazard and increasing time until the next earthquake. *Physical Review E*, *71*. doi:10.1103/PhysRevE.1171.017101.
- Corral, A. (2009). Point-occurrence self-similarity in crackling-noise systems and in other complex systems. *Journal of Statistical Mechanics: Theory and Experiment*. doi:10.1088/1742-5468/2009/1001/P01022.
- Dahlen, F. A., & Tromp, J. (1998). *Theoretical global seismology*. Princeton, New Jersey: Princeton University Press. p. 1025.
- Dahmen, K., Ertas, D., & Ben-Zion, Y. (1998). Gutenberg–Richter and characteristic earthquake behavior in simple mean-field models of heterogeneous faults. *Physical Review E*, *58*, 1494–1501.
- Das, S., & Suhadolc, P. (1996). On the inverse problem for earthquake rupture: the Haskell-type source model. *Journal of Geophysical Research*, *101*, 5725–5738.
- De Blasio, F. V., Ilstad, T., Elverhøi, A., Issler, D., & Harbitz, C. (2004). *High mobility of subaqueous debris flows and the lubricating-layer model*. paper presented at 2004 Offshore Technology Conference, Houston, TX.
- Densmore, A. L., Ellis, M. A., & Anderson, R. S. (1998). Landsliding and the evolution of normal-fault-bounded mountains. *Journal of Geophysical Research*, *103*, 15,203–215,219.

- Dieterich, J. H. (1995). Earthquake simulations with time-dependent nucleation and long-range interactions. *Nonlinear Processes in Geophysics*, 2, 109–120.
- Dieterich, J. H. (2007). Applications of rate- and state-dependent friction to models of fault slip and earthquake occurrence. In H. Kanamori (Ed.), *Treatise on geophysics* (pp. 107–129). Elsevier.
- Dugan, B., & Flemings, P. B. (2000). Overpressure and fluid flow in the New Jersey continental slope: implications for slope failure and cold seeps. *Science*, 289, 288–291.
- Dussauge, C., Grasso, J. R., & Helmstetter, A. (2003). Statistical analysis of rockfall volume distributions: implications for rockfall dynamics. *Journal of Geophysical Research*, 108. doi:10.1029/2001JB000650.
- Dziewonski, A. M., Chou, T.-A., & Woodhouse, J. H. (1981). Determination of earthquake source parameters from waveform data for studies of global and regional seismicity. *Journal of Geophysical Research*, 86, 2825–2852.
- Faccioli, E., Paolucci, R., & Rey, J. (2004). Displacement spectra for long periods. *Earthquake Spectra*, 20, 347–376.
- Farreras, S. F., & Sanchez, A. J. (1991). The tsunami threat on the Mexican west coast: a historical analysis and recommendations for hazard mitigation. *Natural Hazards*, 4, 301–316.
- Feller, W. (1968). *An introduction to probability theory and its applications* (3rd ed.). John Wiley & Sons. p. 509.
- Fukao, Y., & Furumoto, M. (1985). Hierarchy in earthquake size distribution. *Physics of the Earth and Planetary Interiors*, 37, 149–168.
- Fukao, Y. (1979). Tsunami earthquakes and subduction processes near deep-sea trenches. *Journal of Geophysical Research*, 84, 2303–2314.
- Gardner, J. K., & Knopoff, L. (1974). Is the sequence of earthquakes in southern California, with aftershocks removed, Poissonian? *Bulletin of the Seismological Society of America*, 64, 1363–1367.
- Geist, E. L., & Parsons, T. (2006). Probabilistic analysis of tsunami hazards. *Natural Hazards*, 37, 277–314.
- Geist, E. L., & Parsons, T. (2008). Distribution of tsunami inter-event times. *Geophysical Research Letters*, 35, L02612. doi:02610.01029/02007GL032690.
- Geist, E. L., & Parsons, T. (2009). Assessment of source probabilities for potential tsunamis affecting the U.S. Atlantic Coast. *Marine Geology*, 264, 98–108.
- Geist, E. L., & Parsons, T. (2011). Assessing historical rate changes in global tsunami occurrence. *Geophysical Journal International*, 187, 497–509.
- Geist, E. L., Lynett, P. J., & Chaytor, J. D. (2009a). Hydrodynamic modeling of tsunamis from the Currituck landslide. *Marine Geology*, 264, 41–52.
- Geist, E. L., Parsons, T., ten Brink, U. S., & Lee, H. J. (2009b). Tsunami probability. In E. N. Bernard, & A. R. Robinson (Eds.), *The Sea*, Vol. 15 (pp. 93–135). Cambridge, Massachusetts: Harvard University Press.
- Geist, E. L. (1999). Local tsunamis and earthquake source parameters. *Advances in Geophysics*, 39, 117–209.
- Geist, E. L. (2002). Complex earthquake rupture and local tsunamis. *Journal of Geophysical Research*, 107. doi:10.1029/2000JB000139.
- Geist, E. L. (2009). Phenomenology of tsunamis: statistical properties from generation to runup. *Advances in Geophysics*, 51, 107–169.
- Gerstenberger, M., Wiemer, S., & Jones, L. (2004). *Real-time forecasts of tomorrow's earthquakes in California: a new mapping tool*. U.S. Geological Survey Open-File Report 2004-1390 Rep., p. 39.
- Greenhough, J., & Main, I. G. (2008). A Poisson model for earthquake frequency uncertainties in seismic hazard analysis. *Geophysical Research Letters*, 35. doi:10.1029/2008GL035353.

- Gusiakov, V. K. (2001). *Basic Pacific tsunami catalog and database, 47 BC-2000 AD: results of the first stage of the project, paper presented at International Tsunami Symposium*. Seattle, Washington: NOAA.
- Guzzetti, F., Malamud, B. D., Turcotte, D. L., & Reichenbach, P. (2002). Power-law correlations of landslide areas in central Italy. *Earth and Planetary Science Letters*, *195*, 169–183.
- Hainzl, S., Zöller, G., & Scherbaum, F. (2003). Earthquake clusters resulting from delayed rupture propagation in finite fault segments. *Journal of Geophysical Research*, *108*. doi:10.1029/2001JB000610.
- Hainzl, S., Scherbaum, F., & Beauval, C. (2006). Estimating background activity based on interevent-time distribution. *Bulletin of the Seismological Society of America*, *96*, 313–320.
- Hainzl, S., Zöller, G., & Wang, R. (2010). Impact of the receiver fault distribution on aftershock activity. *Journal of Geophysical Research*, *115*. doi:10.1029/2008JB006224.
- Harbitz, C., Parker, G., Elverhøi, A., Marr, J. G., Mohrig, D., & Harff, P. A. (2003). Hydroplaning of subaqueous debris flows and glide blocks: analytical solutions and discussion. *Journal of Geophysical Research*, *108*. doi:10.1029/2001JB001454.
- Harris, R. A., & Simpson, R. W. (1998). Suppression of large earthquakes by stress shadows: a comparison of Coulomb and rate-and-state failure. *Journal of Geophysical Research*, *103*, 24,439–24,451.
- Harris, R. A. (1998). Introduction to special section: stress triggers, stress shadows, and implications for seismic hazard. *Journal of Geophysical Research*, *103*, 24,347–24,358.
- Helmstetter, A., & Sornette, D. (2002). Subcritical and supercritical regimes in epidemic models of earthquake aftershocks. *Journal of Geophysical Research*, *107*. doi:10.1029/2001JB001580.
- Hergarten, S., & Neugebauer, H. J. (1998). Self-organized criticality in a landslide model. *Geophysical Research Letters*, *25*, 801–804.
- Hergarten, S. (2003). Landslides, sandpiles, and self-organized criticality. *Natural Hazards and Earth System Sciences*, *3*, 505–514.
- Hill, B. M. (1975). A simple general approach to inference about the tail of a distribution. *The Annals of Statistics*, *3*, 1163–1174.
- Hillers, G., Carlson, J. M., & Archuleta, R. J. (2009). Seismicity in a model governed by competing frictional weakening and healing mechanisms. *Geophysical Journal International*, *178*, 1363–1383.
- Jankaew, K., Atwater, B. F., Sawai, Y., Choowong, M., Charoentitirat, T., Martin, M. E., et al. (2008). Medieval forewarning of the 2004 Indian Ocean tsunami in Thailand. *Nature*, *455*, 1228–1231.
- Kagan, Y. Y., & Houston, H. (2005). Relation between mainshock rupture process and Omori's law for aftershock moment release rate. *Geophysical Journal International*, *163*, 1039–1048.
- Kagan, Y. Y., & Jackson, D. D. (1991a). Seismic gap hypothesis: ten years after. *Journal of Geophysical Research*, *96*, 21,419–21,431.
- Kagan, Y. Y., & Jackson, D. D. (1991b). Long-term earthquake clustering. *Geophysical Journal International*, *104*, 117–133.
- Kagan, Y. Y., & Jackson, D. D. (1995). New seismic gap hypothesis: five years after. *Journal of Geophysical Research*, *100*, 3943–3959.
- Kagan, Y. Y., & Jackson, D. D. (2011). Global earthquake forecasts. *Geophysical Journal International*, *184*, 759–776.
- Kagan, Y. Y., & Knopoff, L. (1987). Statistical short-term earthquake prediction. *Science*, *236*, 1563–1567.
- Kagan, Y. Y., & Schoenberg, F. (2001). Estimation of the upper cutoff parameter for the tapered Pareto distribution. *Journal of Applied Probability*, *38A*, 158–175.

- Kagan, Y. Y. (1991). Likelihood analysis of earthquake catalogues. *Geophysical Journal International*, 106, 135–148.
- Kagan, Y. Y. (1993). Statistics of characteristic earthquakes. *Bulletin of the Seismological Society of America*, 83, 7–24.
- Kagan, Y. Y. (1996). Comment on "The Gutenberg–Richter of characteristic earthquake distribution, which is it?" by Steven G. Wesnousky. *Bulletin of the Seismological Society of America*, 86, 274–285.
- Kagan, Y. Y. (1997). Seismic moment–frequency relation for shallow earthquakes: regional comparison. *Journal of Geophysical Research*, 102, 2835–2852.
- Kagan, Y. Y. (1999). Universality of the seismic–moment–frequency relation. *Pure and Applied Geophysics*, 155, 537–573.
- Kagan, Y. Y. (2002a). Seismic moment distribution revisited: I. Statistical results. *Geophysical Research Letters*, 148, 520–541.
- Kagan, Y. Y. (2002b). Aftershock zone scaling. *Bulletin of the Seismological Society of America*, 92, 641–655.
- Kagan, Y. Y. (2002c). Seismic moment distribution revisited: II. Moment conservation principle. *Geophysical Research Letters*, 149, 731–754.
- Kagan, Y. Y. (2010). Statistical distributions of earthquake numbers: consequence of branching process. *Geophysical Journal International*, 180, 1313–1328.
- Kanamori, H., & Kikuchi, M. (1993). The 1992 Nicaragua earthquake: a slow earthquake associated with subducted sediments. *Nature*, 361, 714–716.
- Kanamori, H. (1972). Mechanism of tsunami earthquakes. *Physics of the Earth and Planetary Interiors*, 6, 346–359.
- Kayen, R. E., & Ozaki, R. (2002). *Displacement of sloping ground under bi-directional seismic loads, paper presented at seventh U.S. National Conference on Earthquake Engineering (7NCEE)*. Boston, Massachusetts: Earthquake Engineering Research Institute.
- Keefer, D. K. (1984). Landslides caused by earthquakes. *Geological Society of America Bulletin*, 95, 406–421.
- Keefer, D. K. (1994). The importance of earthquake–induced landslides to long-term slope erosion and slope–failure hazards in seismically active regions. *Geomorphology*, 10, 265–284.
- Kempthorne, O., & Folks, L. (1971). *Probability, statistics, and data analysis*. Ames, Iowa: Iowa State University Press. p. 555.
- Kijko, A., & Sellevoll, M. A. (1989). Estimation of earthquake hazard parameters from incomplete data files. Part I. Utilization of extreme and complete catalogs with different threshold magnitudes. *Bulletin of the Seismological Society of America*, 79, 645–654.
- Kijko, A., & Sellevoll, M. A. (1992). Estimation of earthquake hazard parameters from incomplete data files. Part II. Incorporation of magnitude heterogeneity. *Bulletin of the Seismological Society of America*, 82, 120–134.
- Kokusho, T. (1999). Water film in liquefied sand and its effect on lateral spread. *Journal of Geotechnical and Geoenvironmental Engineering, ASCE*, 125, 817–826.
- Korycansky, D. G., & Lynett, P. J. (2005). Offshore breaking of impact tsunamis: the Van Dorn effect revisited. *Geophysical Research Letters*, 32. doi:10.1029/2004GL021918.
- Kreemer, C., Holt, W. E., & Haines, A. J. (2002). The global moment rate distribution within plate boundary zones. In S. Stein, & J. T. Freymueller (Eds.), *Plate boundary zones* (pp. 173–202). Washington, D.C: American Geophysical Union, Geodynamic series.
- Lay, T., Kanamori, H., & Ruff, L. J. (1982). The asperity model and the nature of large subduction zone earthquakes. *Earthquake Prediction Research*, 1, 3–71.
- Lee, H. J., Locat, J., Dartnell, P., Minasian, D., & Wong, F. (2000). *A GIS-based regional analysis of the potential for shallow-seated submarine slope failure, paper presented at Proceedings of the 8th International Symposium on Landslides, Cardiff, Wales*.

- Lee, H. J. (2009). Timing of occurrence of large submarine landslides on the Atlantic ocean margin. *Marine Geology*, 53–64.
- Lennartz, S., Bunde, A., & Turcotte, D. L. (2011). Modelling seismic catalogues by cascade models: do we need long-term magnitude correlations? *Geophysical Journal International*, 184, 1214–1222.
- Leonard, T., Papasouliotis, O., & Main, I. G. (2001). A Poisson model for identifying the characteristic size effects in frequency data: application to frequency-size distributions for global earthquakes, "starquakes", and fault lengths. *Journal of Geophysical Research*, 106, 13,473–413,484.
- Liu-Zeng, J., Heaton, T. H., & DiCaprio, C. (2005). The effect of slip variability on earthquake slip-length scaling. *Geophysical Journal International*, 162, 841–849.
- Locat, J., & Lee, H. J. (2002). Submarine landslides: advances and challenges. *Canadian Geotechnical Journal*, 39, 193–212.
- Longuet-Higgins, M. S. (1952). On the statistical distribution of the heights of sea waves. *Journal of Marine Research*, 11, 245–266.
- Main, I. (1995). Earthquakes as critical phenomena: implications for probabilistic seismic hazard analysis. *Bulletin of the Seismological Society of America*, 85, 1299–1308.
- Main, I. (2000a). A damage mechanics model for power-law creep and earthquake aftershock and foreshock sequences. *Geophysical Journal International*, 142, 151–161.
- Main, I. (2000b). Apparent breaks in scaling in the earthquake cumulative frequency–magnitude distribution: fact or artifact? *Bulletin of the Seismological Society of America*, 90, 86–97.
- Malamud, B. D., Turcotte, D. L., Guzzetti, F., & Reichenbach, P. (2004). Landslide inventories and their statistical properties. *Earth Surface Processes and Landforms*, 29, 687–7111.
- Marsan, D., & Nalbant, S. S. (2005). Methods for measuring seismicity rate changes: a review and a study of how the M_w 7.3 Landers earthquake affected the aftershock sequence of the M_w 6.1 Joshua Tree earthquake. *Pure and Applied Geophysics*, 2005, 1151–1185.
- Martel, S. J. (2004). Mechanics of landslide initiation as a shear fracture phenomenon. *Marine Geology*, 203, 319–339.
- Matthews, M. V., & Reasenber, P. A. (1988). Statistical methods for investigating quiescence and other temporal seismicity patterns. *Pure and Applied Geophysics*, 126, 357–372.
- Matthews, M. V., Ellsworth, W. L., & Reasenber, P. A. (2002). A Brownian model for recurrent earthquakes. *Bulletin of the Seismological Society of America*, 92, 2233–2250.
- McCann, W. R., Nishenko, S. P., Sykes, L. R., & Krause, J. (1979). Seismic gaps and plate tectonics: seismic potential for major boundaries. *Pure and Applied Geophysics*, 117, 1082–1147.
- Micallef, A., Berndt, C., Masson, D. G., & Stow, D. A. V. (2008). Scale invariant characteristics of the Storegga slide and implications for large-scale submarine mass movements. *Marine Geology*, 247, 46–60.
- Mofjeld, H. O. (2009). Tsunami measurements. In E. N. Bernard, & A. R. Robinson (Eds.), *The sea* (pp. 201–235). Cambridge, MA: Harvard University Press.
- Molchan, G., & Kronrod, T. (2009). The fractal description of seismicity. *Geophysical Journal International*, 179, 1787–1799.
- Newman, M. E. J. (2005). Power laws, Pareto distributions and Zipf's law. *Contemporary Physics*, 46, 323–351.
- Newmark, N. M. (1965). Effects of earthquakes on dams and embankments. *Geotechnique*, 15, 139–160.
- Nishenko, S. P., & Buland, R. (1987). A generic recurrence interval distribution for earthquake forecasting. *Bulletin of the Seismological Society of America*, 77, 1382–1399.

- Nishenko, S. P. (1991). Circum-Pacific seismic potential: 1989–1999. *Pure and Applied Geophysics*, 135, 169–259.
- Ogata, Y., & Abe, K. (1991). Some statistical features of the long-term variation of the global and regional seismic activity. *International Statistical Review*, 59, 139–161.
- Ogata, Y., & Zhuang, J. (2006). Space–time ETAS models and an improved extension. *Tectonophysics*, 413, 13–23.
- Ogata, Y. (1988). Statistical models for earthquake occurrences and residual analysis for point processes. *Journal of the American Statistical Association*, 83, 9–27.
- Ogata, Y. (1998). Space–time point–process models for earthquake occurrences. *Annals of the Institute of Statistical Mathematics*, 50, 379–402.
- Ogata, Y. (1999). Estimating the hazard of rupture using uncertain occurrence times of paleoearthquakes. *Journal of Geophysical Research*, 104, 17,995–918,014.
- Okal, E. A. (1988). Seismic parameters controlling far–field tsunami amplitudes: a review. *Natural Hazards*, 1, 67–96.
- Okubo, P. G., & Aki, K. (1987). Fractal geometry of the San Andreas fault system. *Journal of Geophysical Research*, 92, 345–355.
- Ouillon, G., Castaing, C., & Sornette, D. (1996). Hierarchical geometry of faulting. *Journal of Geophysical Research*, 101, 5477–5487.
- Ozaki, R., Takada, S., & Kayen, R. E. (2001). Multi-directional newmark sliding analysis with compliant materials. *Journal of Structural Engineering*, 47A, 571–578.
- Page, M. T., Custódio, S., Archuleta, R. J., & Carlson, J. M. (2009). Constraining earthquake source inversions with GPS data: 1. Resolution-based removal of artifacts. *Journal of Geophysical Research*, 114. doi:10.1029/2007JB005449.
- Parsons, T., & Geist, E. L. (2009). Is there a basis for preferring characteristic earthquakes over a Gutenberg–Richter distribution in probabilistic earthquake forecasting? *Bulletin of the Seismological Society of America*, 99, 2012–2019.
- Parsons, T., & Velasco, A. A. (2009). On near-source earthquake triggering. *Journal of Geophysical Research*, 114. doi:10.1029/2008JB006277.
- Parsons, T., & Velasco, A. A. (2011). Absence of remotely triggered large earthquakes beyond the main shock region. *Nature Geoscience*, 4, 312–316.
- Parsons, T., Ogata, Y., Zhuang, J., & Geist, E. L. (2012). Evaluation of static stress change forecasting with prospective and blind tests. *Geophysical Journal International*, 188, 1425–1440.
- Parsons, T. (2002). Global Omori law decay of triggered earthquakes: large aftershocks outside the classical aftershock zone. *Journal of Geophysical Research*, 107, 2199. doi:2110.1029/2001JB000646.
- Parsons, T. (2008a). Earthquake recurrence on the south Hayward fault is most consistent with a time dependent, renewal process. *Geophysical Research Letters*, 35. doi:10.1029/2008GL035887.
- Parsons, T. (2008b). Monte Carlo method for determining earthquake recurrence parameters from short paleoseismic catalogs: example calculations for California. *Journal of Geophysical Research*, 113. doi:10.1029/2007JB004998.
- Pelayo, A. M., & Wiens, D. A. (1992). Tsunami earthquakes: slow thrust–faulting events in the accretionary wedge. *Journal of Geophysical Research*, 97, 15,321–315,337.
- Pérez, O. J., & Scholz, C. H. (1984). Heterogeneities of the instrumental seismicity catalog (1904–1980) for strong shallow earthquakes. *Bulletin of the Seismological Society of America*, 74, 669–686.
- Polet, J., & Kanamori, H. (2000). Shallow subduction zone earthquakes and their tsunami-migenic potential. *Geophysical Journal International*, 142, 684–702.
- Power, W. L., & Tullis, T. E. (1991). Euclidean and fractal models for the description of rock surface roughness. *Journal of Geophysical Research*, 96, 415–424.
- Prejean, S. H., Hill, D. P., Brodsky, E. E., Hough, S. E., Johnston, M. J. S., Malone, S. D., et al. (2004). Remotely triggered seismicity on the United States West Coast following

- the M_w 7.9 Denali fault earthquake. *Bulletin of the Seismological Society of America*, *94*, S348–S359.
- Rabinovich, A. B. (1997). Spectral analysis of tsunami waves: separation of source and topography effects. *Journal of Geophysical Research*, *102*, 663–612,676.
- Reasenber, P. A., & Simpson, R. W. (1992). Response of regional seismicity to the static stress change produced by the Loma Prieta earthquake. *Science*, *255*, 1687–1690.
- Rice, J. R. (1993). Spatio-temporal complexity of slip on a fault. *Journal of Geophysical Research*, *98*, 9885–9907.
- Rodriguez, C. E., Bommer, J. J., & Chandler, R. J. (1999). Earthquake-induced landslides: 1980–1997. *Soil Dynamics and Earthquake Engineering*, *18*, 325–346.
- Romanowicz, B. (1994). Comment on "A reappraisal of large earthquake scaling" by C. Scholz. *Bulletin of the Seismological Society of America*, *84*, 1675–1676.
- Rong, Y., Jackson, D. D., & Kagan, Y. Y. (2003). Seismic gaps and earthquakes. *Journal of Geophysical Research*, *108*. ESE 6-1–6-14.
- Saichev, A., & Sornette, D. (2007). Theory of earthquake recurrence times. *Journal of Geophysical Research*, *112*. doi:10.1029/2006JB004536.
- Satake, K., & Imamura, F. (1995). Introduction to "Tsunamis: 1992–94. *Pure and Applied Geophysics*, *145*, 373–379.
- Satake, K. (2007). Tsunamis, in *Treatise on Geophysics*. In H. Kanamori, & G. Schubert (Eds.), *Volume 4-Earthquake Seismology* (pp. 483–511). Elsevier.
- Schoenberg, F. P., Brillinger, D. R., & Guttorp, P. (2002). Point processes, spatial-temporal. In A. H. El-Shaarawi, & W. W. Piegorisch (Eds.), *Encyclopedia of environmetrics* (pp. 1573–1577). Chichester: John Wiley & Sons.
- Scholz, C. H. (1994). A reappraisal of large earthquake scaling. *Bulletin of the Seismological Society of America*, *84*, 215–218.
- Selva, J., & Marzocchi, W. (2005). Variations of southern California seismicity: empirical evidence and possible physical causes. *Journal of Geophysical Research*, *110*. doi:10.1029/2004JB003494.
- Shaw, B. E., & Scholz, C. H. (2001). Slip-length scaling in large earthquakes: observations and theory and implications for earthquake physics. *Geophysical Research Letters*, *28*, 2995–2998.
- Shaw, B. E., & Wesnousky, S. G. (2008). Slip-length scaling in large earthquakes: the role of deep-penetrating slip below the seismogenic layer. *Bulletin of the Seismological Society of America*, *98*, 1633–1641.
- Silverman, B. W. (1998). *Density estimation for statistics and data analysis* (6th ed.). Boca Raton, Florida: Chapman and Hall/CRC. p. 175.
- Sornette, D., & Sornette, A. (1999). General theory of the modified Gutenberg–Richter law for large seismic moments. *Bulletin of the Seismological Society of America*, *89*, 1121–1130.
- Sornette, D. (2004). *Critical phenomena in natural sciences* (2nd ed.). Berlin: Springer-Verlag. p. 528.
- Stark, C. P., & Hovius, N. (2001). The characterization of landslide size distributions. *Geophysical Research Letters*, *28*, 1091–1094.
- Stegmann, S., Strasser, M., Anselmetti, F., & Kopf, A. (2007). Geotechnical in situ characterization of subaquatic slopes: the role of pore pressure transients versus frictional strength in landslide initiation. *Geophysical Research Letters*, *34*. doi:10.1029/2006GL029122.
- Stein, R. S. (1999). The role of stress transfer in earthquake occurrence. *Nature*, *402*, 605–609.
- Stigall, J., & Dugan, B. (2010). Overpressure and earthquake initiated slope failure in the Ursa region, northern Gulf of Mexico. *Journal of Geophysical Research*, *115*. doi:10.1029/2009JB006848.

- ten Brink, U. S., Geist, E. L., & Andrews, B. D. (2006). Size distribution of submarine landslides and its implication to tsunami hazard in Puerto Rico. *Geophysical Research Letters*, *33*. doi:10.1029/2006GL026125.
- ten Brink, U. S., Lee, H. J., Geist, E. L., & Twichell, D. (2009a). Assessment of tsunami hazard to the U.S. Atlantic Coast using relationships between submarine landslides and earthquakes. *Marine Geology*, *264*, 65–73.
- ten Brink, U. S., Barkan, R., Andrews, B. D., & Chaytor, J. D. (2009b). Size distributions and failure initiation of submarine and subaerial landslides. *Earth and Planetary Science Letters*, *287*, 31–42.
- Tsuji, Y., Imamura, F., Matsutomi, H., Synolakis, C. E., Nanang, P. T., Jumadi, S., et al. (1995). Field survey of the east Java earthquake and tsunami of June 3, 1994. *Pure and Applied Geophysics*, *144*, 839–854.
- Turcotte, D. L., Holliday, J. R., & Rundle, J. B. (2007). BASS, and alternative to ETAS. *Geophysical Research Letters*, *34*. doi:10.1029/2007GL029696.
- Udwadia, F. E., & Trifunac, M. D. (1974). Characterization of response spectra through the statistics of oscillator response. *Bulletin of the Seismological Society of America*, *64*, 205–219.
- Utsu, T. (1984). Estimation of parameters for recurrence models of earthquakes. *Bulletin of the Earthquake Research Institute*, *59*, 53–66.
- Utsu, T. (2003). Statistical features of seismicity. In W. H. K. Lee, H. Kanamori, P. C. Jennings, & C. Kisslinger (Eds.), *International handbook of earthquake & engineering seismology, part B* (pp. 719–732). Academic Press.
- van Dorn, W. G. (1984). Some tsunami characteristic deducible from tide records. *Journal of Physical Oceanography*, *14*, 353–363.
- Velasco, A. A., Hernandez, S., Parsons, T., & Pankow, K. (2008). Global ubiquity of dynamic earthquake triggering. *Nature Geoscience*, *1*, 375–379.
- Vere-Jones, D. (1976). A branching model for crack propagation. *Pure and Applied Geophysics*, *114*, 711–725.
- Vere-Jones, D. (2010). Foundations of statistical seismology. *Pure and Applied Geophysics*, *167*, 645–653.
- Viesca, R. C., & Rice, J. R. (2010). Modeling slope instability as shear rupture propagation in a saturated porous medium. In D. C. Mosher, C. Shipp, L. Moscardelli, J. Chaytor, C. Baxter, & H. J. Lee, et al. (Eds.), *Submarine mass movements and their consequences IV* (pp. 215–225). Heidelberg, Germany: Springer.
- Wang, Q., Jackson, D. D., & Zhuang, J. (2010a). Missing links in earthquake clustering models. *Geophysical Research Letters*, *37*. doi:10.1029/2010GL044858.
- Wang, Q., Jackson, D. D., & Zhuang, J. (2010b). Are spontaneous earthquakes stationary in California? *Journal of Geophysical Research*, *115*. doi:10.1029/2009JB007031.
- Ward, S. N. (1980). Relationships of tsunami generation and an earthquake source. *Journal of Physics of the Earth*, *28*, 441–474.
- Watanabe, H. (1972). Statistical studies on the wave-form and maximum height of large tsunamis. *Journal of the Oceanographical Society of Japan*, *28*, 229–241.
- Wesnousky, S. G. (1994). The Gutenberg–Richter or characteristic earthquake distribution, which is it? *Bulletin of the Seismological Society of America*, *84*, 1940–1959.
- West, M., Sánchez, J. J., & McNutt, S. R. (2005). Periodically triggered seismicity at Mount Wrangell, Alaska, after the Sumatra earthquake. *Science*, *308*, 1144–1146.
- Yamada, M., Olsen, A. H., & Heaton, T. H. (2009). Statistical features of short-period and long-period near-source ground motions. *Bulletin of the Seismological Society of America*, *99*, 3264–3274.
- Yamashita, T. (1999). Pore creation due to fault slip in a fluid-permeated fault zone and its effect on seismicity: generation mechanism of earthquake swarm. *Pure and Applied Geophysics*, *155*, 625–647.

- Zhuang, J., Christophersen, A., Savage, M. K., Vere-Jones, D., Ogata, Y., & Jackson, D. D. (2008). Differences between spontaneous and triggered earthquakes: their influences on foreshock probabilities. *Journal of Geophysical Research*, *113*. doi:10.1029/2008JB005579.
- Zöller, G., Holschneider, M., & Ben-Zion, Y. (2004). Quasi-static and quasi-dynamic modeling of earthquake failure at intermediate scales. *Pure and Applied Geophysics*, *161*, 2103–2118.